DOE/PC/92104--T15

92PC92104-TPR-15

ADVANCED THERMALLY STABLE JET FUELS

Technical Progress Report
January - March 1996

H.H. Schobert. S. Eser. C. Song. P.G. Hatcher. A. Boehman. M.M. Coleman

Contributions from:

J. Bortiatynski. W.-C. Lai. S. Martin. D. McKinney. M. Tercha.
J. Yu. P. Sanghani. M. Sobkowiak.

August 1996

Prepared for U.S. Department of Energy
under
Contract No. DE-FG22-92PC92104

PENNSTATE

College of Earth and
Mineral Sciences

92PC92104-TPR-15

ADVANCED THERMALLY STABLE JET FUELS

Technical Progress Report
January - March 1996

H.H. Schobert, S. Eser, C. Song, P.G. Hatcher, A. Boehman, M.M. Coleman

Contributions from:

J. Bortiatynski, W.-C. Lai, S. Martin, D. McKinney, M. Tercha,
J. Yu, P. Sanghani, M. Sobkowiak,

August 1996

Prepared for U.S. Department of Energy
under
Contract No. DE-FG22-92PC92104

DISCLAIMER

OBJECTIVES i

SUMMARY ii

TECHNICAL PROGRESS 1

Task 1. Investigation of the Quantitative Degradation Chemistry of Fuels 1

1. Reactive Structure Index for Correlation of High Temperature Thermal Stability of Saturated Hydrocarbons (Contributed by Wei-Chuan Lai and Chunshan Song) 1
2. Thermal Decomposition of n-Butylbenzene in Near-Critical and Supercritical Regions: Product Distributions and Reaction Mechanisms (Contributed by Jian YU and Semih Eser) 10
3. Thermal Degradation Studies of ^{13}C-labeled Dodecane Mixed with a Petroleum Derived Jet Fuel, JP-8P, Using Gas Chromatography-Select Ion Monitoring. (Contributed by Daniel E. McKinney, Jacqueline M. Bortiatynski, and Patrick G. Hatcher 17

Task 2. Investigation of Incipient Deposition 23

1. Deposit Growth During Heating of Coal Derived Aviation Gas Turbine Fuels. (Contributed by Prashant C. Sanghani and André Boehman) 23
2. Modeling Heat Transfer to Flowing Jet fuels (Contributed by Mark A. Tercha and André L. Boehman) 26

Task 4. Coal-Based Fuel Stabilization Studies 28

1. Towards the Design of Thermally Stable Jet Fuels at Both Moderate (<250°C) and High (>400°C) Temperatures. (Contributed by Maria Sobkowiak and Michael M. Coleman) 28

Task 5. Exploratory Studies on the Direct Conversion of Coal to High-Quality Jet Fuels 30

1. Contribution of Mineral Matter to Low Temperature Liquefaction Mechanisms.(Contributed by Shona Martin) 30

Appendix I. Tables 43

Appendix II. Figures 53

Appendix III Figures from #14 72

OBJECTIVES

The Penn State program in advanced thermally stable jet fuels has five components: 1) development of mechanisms of degradation and solids formation; 2) quantitative measurement of growth of sub-micrometer and micrometer-sized particles during thermal stressing; 3) characterization of carbonaceous deposits by various instrumental and microscopic methods; 4) eludication of the role of additives in retarding the formation of carbonaceous solids; and 5) assessment of the potential of producing high yields of cycloalkanes and hydroaromatics by direct liquefaction of coal.

SUMMARY

A reactive structure index was developed to correlate the molecular structures of saturated hydrocarbons with their reactivities using a linear group contribution method. The index is composed of several sub-indices determined from the structure, including carbon group indices, ring index, and conformation index. The effects on decomposition of ring structure, side-chain length, steric isomers, and branching were examined. Good correlations were obtained for two sets of saturated hydrocarbons.

The reactivity of alkanes and cycloalkanes increases with increasing chain or side-chain length. Cycloalkanes are desirable components of advanced jet fuels, in terms of having higher thermal stability and density than *n*-alkanes of the same carbon number. The *cis*-isomer is usually more reactive than the *trans*-isomer, except for *cis*-1,3-dimethylcyclohexane, which is more stable than its *trans*-isomer. The presence of a branch or branches appears to decrease the decomposition rate compared to *n*-alkanes.

The thermal decomposition of *n*-butylbenzene was studied in the near-critical and supercritical regions as a function of pressure, temperature, and conversion. Thermal stressing experiments were carried out in a Pyrex glass tube reactor with a total volume of 45–50 mL. Using a sealed glass tube eliminates the concerns for temperature variations and possible catalytic effects of metal surfaces in the reactor, as encountered in our standard microautoclave ("tubing bomb") reactors during thermal treatment.

Gas chromatography-select ion monitoring in combination with carbon-13 labeling has been demonstrated as an excellent technique for monitoring the thermal degradation of 6-^{13}C-dodecane in JP-8P. Using this technique, one can discriminate between naturally occurring unlabeled dodecane in the system to carbon-13 added, by differences in their molecular weights.

Work has continued on the development of a global kinetic scheme to describe the formation of deposits. In addition, work was initiated on modeling heat transfer to flowing jet fuels using an entry-length heat and mass transfer model for flow in tubes. This was undertaken to provide a modeling basis for future work in flowing reactor systems at Penn State.

Experiments have been initiated to examine the prospects of stabilizing fuels at both moderate temperatures, below 250°C, and high temperatures, above 400°C. Systematic experiments are underway to investigate the reactions of dodecane with tetrahydroquinoline additive and of Jet A-1 with added tetrahydroquinoline or benzyl alcohol.

Wyodak subbituminous coal shows higher overall conversions at relatively mild conditions (350°C) when demineralized. This suggests that there is no mineral matter catalysis of hydrogen donation. Work is continuing on identifying the mineral phases or species contributing to possible low-temperature hydrogenation mechanisms.

For hydrogenation of naphthalene in *n*-tridecane at 200°C, both platinum and palladium catalysts supported on MCM-41 zeolite are substantially more active than the corresponding catalysts supported on alumina or titania. Both Pt/MCM-41 and Pd/MCM-41 catalysts promoted hydrogenation to completion, so that the dominant products are *trans*- and *cis*-decalin, whereas tetralin is still one of the major products with both alumina and titania-supported catalysts. Palladium catalysts showed higher selectivity to *trans*-decalin, whereas higher selectivity to *cis*-decalin was afforded by platinum catalysts. The selectivity to decalin isomers also depends on the support and metal type. Among the three supports, MCM-41 gives the highest *trans-/cis-* ratio. Between the two metals, palladium gives the higher *trans-/cis-* ratio.

Task 1. Investigation of the Quantitative Degradation Chemistry of Jet Fuels

1. Reactive Structure Index for Correlation of High Temperature Thermal Stability of Saturated Hydrocarbons (Contributed by Wei-Chuan Lai and Chunshan Song)

Abstract

For the development of advanced jet fuels, it is important to examine how the structure of various (jet fuel range) hydrocarbons affects their thermal stability at temperatures above 400 °C under elevated pressures. The objective of this section is to develop a reactive structure index (RSI) to correlate the molecular structures of saturated hydrocarbons with their decomposition rate constants using a group contribution method. The effects of ring-structure, side-chain length (up to C_{10}), steric isomers, and branching on the decomposition rate of open-chain alkanes and cycloalkanes were studied at 450 °C under an initial pressure of 0.79-MPa N_2 in batch reactors. The reactivity of alkanes/cycloalkanes increases with increasing chain/side-chain length. Cycloalkanes (≥ 5-membered ring) are more stable than *n*-alkanes with the same carbon number. The *cis* isomer usually decomposes about 3–5 times faster than the *trans* isomer except for *trans*-1,3-dimethylcyclohexane, which decomposes about 2.5 times faster than its *cis*-isomer. The presence of a branch or branches appears to decrease the rate of decomposition as compared to that of the *n*-alkanes. The RSI can be derived by integrating several sub-indices determined from the structure via a simple group contribution method, including carbon group indices, ring index, and conformation index. Good correlations between RSI and rate constant were obtained for two sets of saturated hydrocarbons (38 and 17 compounds, respectively).

Introduction

The thermal stability of jet fuels will play an important role in the development and operation of future high-Mach aircraft, where the fuel is the main coolant to absorb the dramatically increasing heat loads [1-4] and the fuel may be heated to 540 °C or higher [5,6]. Advanced jet fuels are required to mitigate serious pyrolytic degradation of the fuels and subsequent formation of solid deposits on critical aircraft systems at such high temperatures. The future source and composition of advanced fuels remain to be determined. The future fuels may derive from hydrocarbon resources such as petroleum, coal, oil shale, and tar sands. Therefore. for the development of advanced jet fuels, it is

important to examine how the structure of various (jet fuel range) hydrocarbons affects their thermal stability at temperatures above 400 °C under elevated pressures.

The objective of this section is to develop a reactive structure index (RSI) to correlate the molecular structures of saturated hydrocarbons with their activities using a group contribution method. The concept of group contribution is not at all new. Group contribution has been applied to the estimation of thermochemical data [7] and to studying the effect of side-chain length of cyclohexanes on their decomposition rate [8]. The correlation, for reactions of cycloalkanes at 427 °C, became less reliable for alkyl side chains exceeding C_4 in length [8]. Correlation between the apparent rate constants of *n*-alkanes at 500 °C and 1 atm with carbon number was also reported in literature [9]. What is new in this work is that we have developed a reactive structure index (RSI) system incorporating the effects of ring structure, side-chain length (up to C_{10}), steric isomers, and length and branching on the reactivity of open-chain alkanes and cycloalkanes. The pyrolysis experiments were carried out in or near the supercritical region, which is relevant to the anticipated environments in future high-Mach jet aircraft.

Experimental

In total, 38 reagent-grade hydrocarbons were used in this study. Classes of compounds studied are (a) *n*-alkanes (C_mH_{2m+2}, m = 5-12, 14, 16), (b) branched alkanes including 2,2,4-trimethylpentane, 2,2,5-trimethylhexane, 3-methylundecane, and 2,2,4,6,6-pentamethylheptane, (c) cycloalkanes including cyclohexane, seven *n*-alkylcyclohexanes (alkyl side-chain = C_mH_{2m+1}, m = 1, 2, 3, 4, 6, 8, 10), isopropylcyclohexane, isobutylcyclohexane, *tert*-butylcyclohexane, cyclopentane, and methylcyclopentane, (d) bicyclics including dicyclohexyl, 1,2-dicyclohexylethane, and dicyclopentyl, (e) steric (*trans*- and *cis*-) isomers including 1,2-dimethylcyclohexane (DMCH), 1,3-DMCH, 1,4-DMCH, and decahydronaphthalene (decalin). The chemicals were obtained from Aldrich Chemical Company, K&K Laboratories, or TCI America, and were used as received.

Pyrolytic reactions were performed in 23.2-mL stainless steel tubing bomb reactors at 450 °C for a heating period of 21–480 min under an initial pressure of 0.79 MPa UHP-N_2. The reactor was loaded with 5-mL sample and leak-tested. To ensure an inert environment and minimize oxidation reactions, the sealed reactor was purged repetitively (six times) with 6.9 MPa UHP-N_2 to remove air and dissolved oxygen in the sample. The reactor was then pressurized to 0.79 MPa with UHP-N_2 before being immersed into a fluidized sand bath preheated to 450 °C. After the reaction, the reactor was quenched in a cold water bath and the gaseous and liquid products were carefully collected. The gaseous products were

quantitatively analyzed using a Perkin-Elmer Autosystem GC equipped with two detectors, a thermal conductivity detector (TCD) and a flame ionization detector (FID). The liquid products were analyzed on an HP 5890II GC coupled with an HP 5971A Mass Selective Detector and quantified by a Perkin-Elmer GC 8500 equipped with an FID. More analytical details may be found elsewhere [10].

Results and Discussion

The pseudo-first-order rate constants of hydrocarbons at elevated pressure were chosen as the measure of their reactivities. Pyrolysis at 450 °C was approximated by a first-order relation as shown in Equation 1

$$-\frac{dC}{dt} = k\ C \tag{1}$$

where C is the reactant concentration (mol/cm^3), t is the reaction time (h), and k is the first-order rate constant (h^{-1}). The first-order rate constant can be derived from reactant conversion (X) as shown in Equation 2.

$$k = \frac{1}{t} \ln \frac{1}{1 - X} \tag{2}$$

Figure 1 shows the changes of rate constant with total carbon number (TCN) in normal alkanes and normal alkylated cyclohexanes (*n*-ACH). The decomposition rate of *n*-alkanes/ACH increases with increasing chain/side-chain length. The overall decomposition rate for *n*-alkanes and *n*-ACH could be represented by a linear function of TCN over the entire carbon number range studied except for cyclohexane and methylcyclohexane. This observation indicates that *n*-ACH with long side chains reacted like *n*-alkanes. The general reaction mechanism of *n*-alkanes is characterized by radical mechanisms involving initiation, hydrogen abstraction, radical isomerization such as 1,5- and 1,4-shift isomerization, radical decomposition, radical addition, and termination [10]. The product distribution from *n*-ACH showed that the major reaction pathways of *n*-ACH strongly depend on the side-chain length. For *n*-ACH with side-chain length ≥ 3, the major reaction at early decomposition stage is β-scission leading to C-C bond cleavage in the side-chain at or near the ring followed by H-abstraction. This in a sense is similar to the reaction mechanism of *n*-alkanes. Besides, under the conditions used, *n*-alkylcyclohexanes do not undergo ring-opening cracking to any significant extent. As for cyclohexane and methylcyclohexane, the dominant reaction is isomerization to form alkylcyclopentanes via ring-contraction. In short, although these compounds differ widely in structure, they can all be constructed from a small number of functional groups, and their decomposition mechanisms display some similarities. Therefore, the concept of linear group contribution

may be applicable to the estimation of compound reactivity. For example, the reactivities of *n*-alkanes and *n*-ACH may be incorporated into and illustrated by a reactive structure index by the introduction of a ring index.

n-Alkylcyclohexanes are more stable than *n*-alkanes with the same total carbon number. The TCN difference is about 3 when *n*-ACH and *n*-alkanes have similar decomposition extent at 450 °C (Figure 1). For example, *n*-hexylcyclohexane (TCN = 12) and *n*-nonane (TCN = 9) have similar rate constant and their TCN difference is 3. It was speculated that there are three factors that might account for the higher stability of cycloalkanes than *n*-alkanes [11]. The first is that the initiation reaction of the former is much more difficult than that of the latter. The second factor is that the β-scission of a cyclohexyl radical is more difficult than that of a secondary alkyl radical. This arises from the difficulty of orbital overlapping required for C=C bond formation in the β-scission of cyclohexyl radical, as compared to the more flexible alkyl radical. The third factor is that the intermediate products of *n*-ACH, cyclohexenes, serve as radical scavengers which inhibit further decomposition. Therefore, it is desirable to have cycloalkanes rather than *n*-alkanes for fuel stability consideration at high temperatures; in addition, the fact that cycloalkanes have greater calorific values per unit volume than *n*-alkanes also indicates that cycloalkanes are desirable components of high-density jet fuels.

Figure 2 compares the rate constants of compounds with 5-membered and 6-membered ring. It shows that the former are more stable than the latter. For example, cyclopentane is more stable than cyclohexane, methylcyclopentane is more stable than methylcyclohexane, and dicyclopentyl is more stable than dicyclohexyl. However, it should be noted that methylcyclopentane is more reactive than cyclohexane (both with the same TCN, 6). Lower stability with the former is due in part to the easier β-scission of methylcyclopentyl radical (C-C bond cleavage in the side-chain at the ring) compared to that of cyclohexyl radical (C-H bond cleavage in the ring). Figure 3 shows the rate constants of three sets of isomers (normal and branched alkanes). The presence of a branch or branches appears to decrease the rate of decomposition as compared to that of the *n*-alkanes. Note that *n*-alkanes contain only two groups of carbons, i.e., primary [$-CH_3-(C)$] and secondary [$-CH_2-(C)_2$]. An *n*-alkane of TCN equivalent to *m* contains 2 primary and *m*-2 secondary carbon groups; each additional [$-CH_2-(C)_2$] group will increase the TCN by one. On the other hand, branched alkanes may be composed of four groups: tertiary [$-CH-(C)_3$] and quaternary [$-C-(C)_4$] as well as primary and secondary carbons. Therefore, Figure 3 implies that the overall decomposition rate is a function of both TCN and the types of carbons in the alkanes, in other words, depending on whether a carbon atom is primary, secondary, tertiary, or quaternary. Figure 4 presents the decomposition rates of four pairs

of steric isomers. The *cis* isomer usually decomposes about 3–5 times faster than the *trans* isomer. One exception shown here is that *trans*-1,3-DMCH decomposes about 2.5 times faster than its *cis*-isomer.

In summary, the above results indicate that RSI may be derived by integrating several structure sub-groups determined from the structure via a simple group contribution method, including carbon group index, ring index, and conformation index. We found that the RSI can be derived by a simple linear combination of six sub-group indices, as shown in Equation 3,

$$RSI = \sum_{j=1}^{6} a_j I_j \tag{3}$$

where a_j (j=1,...,6) are the number of sub-groups j, I_j (j=1,...,4) are the carbon group indices including primary, secondary, tertiary, and quaternary, respectively, I_5 is the ring index, and I_6 is the correction index to distinguish the interactions of non-bonded, next-nearest neighbors such as conformational effects and 1,5-H repulsion [7]. There are a number of approximations inherent in Equation 3. First, the carbon groups in alkanes and in the side chain of alkylcycloalkanes were assumed to have the same contribution. In other words, we do not distinguish the differences of carbon groups between alkanes and side chain of alkylcycloalkanes. This is a reasonable assumption to minimize the number of sub-group required. The supporting evidence is given in the above discussion on Figure 1. Second, the isomers with the same degree of branching react at the same rates. For example, Equation 3 will give the same RSI for isomeric species such as monobranched 2-methylnonane and 3-methylnonane, di-branched 2,2-dimethylnonane and 3,3-dimethylnonane, and so on. Third, linear assumptions were used for the entire range studied; therefore, some minor corrections are needed for smaller hydrocarbons such as *n*-pentane and cycloalkanes with TCN = 5 ~7 to account for non-linear behavior.

The pseudo-first-order rate constant (k, a measure of reactivity) depending on the overall RSI, was assumed to follow the linear Equation 4.

$$k = a + b\,(RSI) \tag{4}$$

The constants a and b in Equation 4 and I_j (j=1,....6) in Equation 3 can be determined from the data of 38 model compounds by regression analysis. The values of the sub-indices were empirically determined and are shown in Table 1. A plot of the experimental rate constants as a function of the RSI is shown in Figure 5. The linear relationship at 450 °C is given by Equation 5.

$$k_{pred} = -0.54 + 0.0178\ RSI \quad (5)$$

An example of the calculation of the RSI and the resultant predicted rate constant was given here by using 2,2,4,6,6-pentamethylheptane, for which we can find that there are 7 primary, 2 secondary, 1 tertiary, 2 quaternary carbons, 0 ring structure, and a pair of 1,5 H repulsions. Therefore, RSI equals 7x4+2x10+1x13+2x5+0+2x(-3) = 65, and the predicted rate constant at 450 °C can be calculated from Equation 5, k_{pred} = –0.54+0.0178x(65) = 0.62. The predicted rate constant, 0.62, is close to the experimental one, 0.66. Table 2 presents the calculated RSI results for 34 compounds.

The reliability of the sub-group indices and Equation 5 in predicting rate constants, can be seen from Figure 6, which compares the 38 experimentally measured rate constants at 450 °C to the values predicted from Equation 5. The line corresponding to exact agreement is drawn as a diagonal. It is clear that the predicted values are in good agreement with experimental ones over a wide range (two magnitudes) of decomposition rates. It should be noted that k increases with increasing RSI, but the relationship between k and RSI was not limited to be linear. In fact, the linear relationship given in Equation 5 is just a special case of a more general quadratic relationship.

To further examine the applicability of the sub-group indices and RSI data in different reaction conditions, we performed additional experiments using 17 hydrocarbons in different reactors with larger capacity (28 mL). The 17 hydrocarbons include *trans*-decalin, *n*-alkanes (C_mH_{2m+2}, m = 6-10, 12, 14, 16), cyclohexane, and seven *n*-alkylcyclohexanes (alkyl side-chain = C_mH_{2m+1}, m = 1, 2, 3, 4, 6, 8, 10). The new experiments were carried out with lower effective reaction temperature than 450 °C and smaller reactant concentrations. The results are presented in Figure 7, which shows the experimental rate constants versus the RSI calculated from the sub-indices in Table 1. A quadratic relationship was observed as shown in Equation 6.

$$k_{pred} = -0.144 + 0.00267\ RSI + 6.76\times10^{-5}\ (RSI)^2 \quad (6)$$

These results demonstrate the potential usefulness of RSI in predicting hydrocarbon stability. For example, a relationship like Equations 5 or 6 can be derived with a small number of (four or five) experiments under a certain reaction condition, and then the derived correlation can be used to predict the thermal decomposition rates for a much larger number of compounds under the same reaction conditions. In summary, RSI could be used as a tool to predict thermal stability and to screen potential thermally stable compounds.

In a sense, RSIs are the results from semi-empirical correlation of reactivity data with the molecular structure or properties; there exist some bases for the group indices in Table

1. For instance, there is a qualitative correspondence between the carbon indices, I_j (j=1,2,3), and the predicted relative rates of hydrogen abstraction of these carbon groups. Hydrocarbon decomposition is substantially affected by propagation steps, of which hydrogen abstraction is an essential part in radical mechanisms [10]. Therefore, it is worthwhile to look at the rates of hydrogen abstraction. Based on the kinetic parameters of Ranzi et al. [12], it can be estimated that the relative rates of radical formation by abstracting a hydrogen atom from a primary, secondary, or tertiary carbon at 450 °C are 1:4:16. Taking into account the number of hydrogen atoms available for abstraction in the respective carbon groups, the calculated relative rates of hydrogen abstraction of these carbon groups are (1x3):(4x2):(16x1) or 3:8:16, which is relatively close to that of I_1, I_2, and I_3, i.e., 4:10:13.

Another factor is conformational effect. Transition-state theory shows that

$$\ln (k) = \ln (\frac{k_B T}{h}) + \frac{T\Delta S^{\neq} - \Delta H^{\neq}}{RT} \quad (7)$$

where k_B is Boltzmann's constant, T is absolute temperature in K, h is Planck's constant, $\Delta S^{\neq}$ is the entropy difference between intermediates and reactants, and $\Delta H^{\neq}$ is the enthalpy difference between intermediates and reactants. When subjected to reaction, the less stable isomer (usually *cis*) is mainly converted into the more stable conformational isomer (usually *trans*). Therefore, the rate constant ratio between two conformational isomers could be approximated as shown in Equation 8,

$$\ln (\frac{k_{\text{less stable}}}{k_{\text{more stable}}}) \propto [-\Delta H_{rx}/(RT)] \quad (8)$$

where ΔH_{rx} is the heat of isomerization reaction between the conformational isomers (*cis* and *trans*). Equation 8 implies that the logarithm of the rate constant ratio of conformational isomers is proportional to $-\Delta H_{rx}$. The proportional constant was about 0.75, estimated from the data of four pairs of conformational isomers at 450 °C. In short, the rate constant ratio of conformational isomers at 450 °C is shown as Equation 9.

$$\frac{k_{\text{less stable}}}{k_{\text{more stable}}} = \exp [-0.75\ \Delta H_{rx}/(RT)] \quad (9)$$

The RSI correlation developed in this work for saturated hydrocarbons should also be applicable to aromatic compounds such as alkylated benzenes by introducing a ring index for aromatic ring. This is because these compounds all proceed through radical mechanisms involving similar elementary steps such as initiation, hydrogen abstraction, radical isomerization, radical decomposition, radical addition, and termination. Because of the fundamental nature of the chosen sub-groups such as carbon types, the indices are expected to be valid for many more hydrocarbons. Another benefit of developing RSI based on

carbon types is that the primary, secondary, tertiary, and quaternary carbons of saturated hydrocarbons can be easily distinguished from ^{13}C NMR. Finally, it should be noted that the current RSIs are derived based on reactivity of pure compounds at 450 °C. The RSI results may be only good for reactions near 450 °C, and whether they are directly applicable to a mixture system is less clear. We are currently evaluating these effects.

Conclusions

A reactive structure index was developed to correlate the molecular structures of saturated hydrocarbons with their reactivities using a simple linear group contribution method. The RSI is composed of several sub-indices determined from the structure including carbon group indices, ring index, and conformation index. The effects of ring-structure, side-chain length (up to C_{10}), steric isomers, and branching on decomposition rate were examined. Good correlations between RSI and pseudo-first-order rate constant were obtained for two sets of saturated hydrocarbons (38 and 17 compounds, respectively).

The reactivity of alkanes/cycloalkanes increases with increasing chain/side-chain length. Cycloalkanes (≥ 5-membered ring) are desirable components of advanced jet fuels, in terms of higher stability and density than *n*-alkanes of the same carbon number. The *cis* isomer usually is more reactive than the *trans* isomer except for *cis*-1,3-dimethylcyclohexane, which is more stable than its *trans*-isomer. The presence of a branch or branches appears to decrease the decomposition rate compared to *n*-alkanes.

References

1. Lee, C. M.; Niedzwiecki, R. W. High Speed Commercial Transport Fuels Considerations and Research Needs. *Prepr.-Am. Chem. Soc., Div. Petrol. Chem.* **1989**, *34* (4), 911-919.

2. Moler, J. L.; Steward, E. M. Thermal Decomposition Studies of Jet Fuel Components: Dodecane, Octane, 2-Methylundecane, and Bicyclohexyl. *Prepr.-Am. Chem. Soc., Div. Pet. Chem.* **1989**, *34* (4), 837-840.

3. Roquemore, W. M.; Pearce, J. A.; Harrison III, W. E.; Krazinski, J. L.; Vanka, S. P. Fouling in Jet Fuels: a New Approach. *Prepr.-Am. Chem. Soc., Div. Pet. Chem.* , **1989**, *34* (4), 841-849.

4. Hazlett, Robert N. *Thermal Oxidation Stability of Aviation Turbine Fuels*. ASTM Monograph 1, American Society for Testing and Materials: Philadelphia, PA, **1991**; 163 pp.

5. Edwards, T.; Liberio, P. D. The Relationship between Oxidation and Pyrolysis in Fuels Heated to 590 °C. *Prepr.-Am. Chem. Soc., Div. Pet. Chem.* **1994**, *39* (1), 92-

96.

6 Edwards, T.; Atria, J. V. Deposition from High Temperature Jet Fuels. *Prepr.-Am. Chem. Soc., Div. Pet. Chem.* **1995**, *40* (4), 649-654.

7. Benson, S. W. *Thermochemical Kinetics, Methods for the Estimation of Thermochemical Data and Rate Parameters.* 2nd ed.; Wiley: New York. **1976**.

8. Fabuss, B. M.; Smith, J. O.; Satterfield, C. N. Thermal Cracking of Pure Saturated Hydrocarbons. In *Advances in Petroleum Chemistry and Refining*; McKetta, John J., Ed.; **1964**, Volume 9, pp.156-201. Interscience Publishers: New York.

9. Voge, H. H.; Good, G. M. Thermal Cracking of Higher Paraffins. *J. Am. Chem. Soc.* **1949**, *71,* 593-597.

10. Song, C.; Lai, W.-C.; Schobert, H. H. Condensed-Phase Pyrolysis of *n*-Tetradecane at Elevated Pressures for Long Duration. Product Distribution and Reaction Mechanisms. *Ind. Eng. Chem. Res.* **1994**, *33*, 534-547.

11. Lai, W.-C.; Song, C. Pyrolysis of Alkylcyclohexanes in or near Supercritical Phase. Product Distribution and Reaction Pathways. *Fuel Processing Technology* **1996**, in press.

12. Ranzi, E.; Dente, M.; Pierucci, S.; Biardi, G. Initial Product Distributions from Pyrolysis of Normal and Branched Paraffins. *Ind. Eng. Chem. Fundam.* **1983**, *22*, 132-139.

2. Thermal Decomposition of n-Butylbenzene in Near-Critical and Supercritical Regions: Product Distributions and Reaction Mechanisms (Contributed by Jian Yu and Semih Eser)

Introduction

The results from thermal decomposition of *n*-butylbenzene have been presented in a previous report [1]. That study was focused on higher conversions and a tubing bomb reactor was used for thermal stressing experiments. The experiments were carried out at 450 °C with a sample loading of 5 mL.

In this work, thermal decomposition of *n*-butylbenzene was studied in near-critical and supercritical regions as a function of pressure, temperature, and conversion. Thermal stressing experiments were carried out in a Pyrex glass tube reactor with a total volume of 45–50 mL. Using a sealed glass tube eliminates the concerns for temperature variations in the reactor, as encountered in the tubing bomb reactor, and possible catalytic effects of metal surfaces during thermal treatment.

Results and Discussion

1. Product Distributions. The liquid products from thermal decomposition of *n*-butylbenzene include toluene, styrene, ethylbenzene, benzene, allylbenzene, and tetralin. Also present are some secondary products, including *n*-propylbenzene, isopropylbenzene, *sec*-butylbenzene, isobutylbenzene, *n*-amylbenzene, 1-propylbutylbenzene, 1,3-diphenylpropane, 1,4-diphenylbutane, 1,6-diphenylhexane, and three other C_6-diphenyls. At higher conversions (> 30 %), more than 150 liquid compounds were found.

Figures 8 and 9 show the effects of pressure on product distributions for the thermal decomposition of *n*-butylbenzene at 425 °C for 15 min. The initial reduced pressure ($P_r = P/P_c$) was calculated at the given temperature and loading ratio, defined as the sample volume at room temperature divided by the reactor volume, using Soave-Redlich-Kwong equation of state [2]. The conversions are between 6 and 7 % in the pressure range examined. It can be seen that at lower conversions the major liquid products are toluene and styrene. As pressure increases, the styrene yield decreases and the toluene yield increases. In contrast to a higher yield of styrene in the sub-critical region, a higher toluene yield is obtained in the far supercritical region. It is clear that the high-pressure supercritical conditions suppress the formation of styrene. On the other hand, the yields of ethylbenzene and benzene remain unchanged while that of allylbenzene decreases with the increasing pressure. The yields of secondary products also change with pressure. Figure 9 shows that the yields of all the secondary products, except *n*-propylbenzene, increase with the increasing pressure. Although not shown in Figure 9, the

yields of some other secondary products, such as 1-propylbutylbenzene, 1,6-diphenylhexane, and two other C_6-diphenyls, also increase with the increasing pressure. Under supercritical conditions the major secondary products include *sec*-butylbenzene, 1,3-diphenylhexane, one C_6-diphenyl, and 1,3-diphenylpropane.

Figures 10 and 11 show the effects of temperature on product distributions at similar conversion levels. The conversions are 15.9, 15.8, and 14.7% for three different temperatures: 400, 425, and 450°C, respectively. As temperature increases, the yields of styrene and allylbenzene increase while those of toluene, ethylbenzene, and benzene remain almost unchanged. The yields of most secondary products decrease with the increasing temperature.

Figures 12 and 13 show the effects of conversion on product distributions for the thermal decomposition of *n*-butylbenzene at 425 °C with a loading ratio of 0.36, which corresponds to a initial reduced pressure of 1.87. For 100 moles of reactant converted, the yield of styrene decreases from 26 to 3.5 moles and that of ethylbenzene increases from 4 to 11 moles as the conversion increases from 6.9 to 35.5 %. The yield of toluene slightly increases and that of benzene does not change significantly with the increasing conversion. The allylbenzene yield decreases with the increasing conversion. Among the secondary products, the yields of *sec*-butylbenzene and 1,3-diphenylhexane decrease while those of isobutylbenzene, *n*-propylbenzene, and isopropylbenzene increase with the increasing conversion. The yield of 1,3-diphenylpropane first increases and then decreases while that of 1-propylbutylbenzene first increases and then remains at a stable level as the conversion increases.

2. Reaction Mechanisms. Thermal decomposition of *n*-butylbenzene proceeds by free radical mechanisms. To account for the observed product distributions and the changes in product composition with reaction conditions, the following mechanisms have been suggested for the thermal decomposition of *n*-butylbenzene in the near-critical and supercritical regions.

The reaction products from the thermal decomposition of *n*-butylbenzene include compounds from primary and secondary reactions. The major primary reactions can be described by eqs 1 to 7:

$$C_6H_5CH_2CH_2CH_2CH_3 \rightarrow C_6H_5CH_2\cdot + CH_3CH_2CH_2\cdot \quad (1)$$

$$R\cdot + C_6H_5CH_2CH_2CH_2CH_3 \rightarrow RH + C_6H_5(C_4H_8)\cdot \quad (2)$$

$$C_6H_5\dot{C}HCH_2CH_2CH_3 \rightarrow C_6H_5CH{=}CH_2 + CH_3CH_2\cdot \quad (3)$$

$$C_6H_5CH_2\dot{C}HCH_2CH_3 \rightarrow C_6H_5CH_2CH{=}CH_2 + CH_3\cdot \quad (4)$$

$$C_6H_5CH_2CH_2\dot{C}HCH_3 \rightarrow C_6H_5CH_2\cdot + CH_2{=}CHCH_3 \quad (5)$$

$$C_6H_5CH_2CH_2CH_2CH_2\cdot \rightarrow C_6H_5CH_2CH_2\cdot + CH_2{=}CH_2 \quad (6)$$

$$R_1\cdot + R_2\cdot \rightarrow \text{products} \quad (7)$$

The initiation occurs by homolytic cleavage of the weakest bond in the reactant molecule. Bond dissociation energies can be calculated using the group additivity law suggested by Benson [3]. Table 3 shows the homolytic bond dissociation energies (BDEs) for different C–C and C–H bonds in the *n*-butylbenzene molecule. It can be seen that the weakest bond in the *n*-butylbenzene molecule is the C_α–C_β bond in the side chain since the cleavage of this bond produces the resonance-stabilized benzyl radical. If it is assumed that the differences in activation energies for the dissociation of *n*-butylbenzene into various radical pairs are equal to the differences in BDEs, one would find that at 425 °C the reaction rate for the formation of benzyl radical and 1-propyl radical is at least 10^4 times higher than those for any other bond scission reactions. Therefore, the initiation reaction occurs predominately by eq 1.

The radicals formed from the initiation reaction would abstract hydrogen atoms from *n*-butylbenzene to form four butylbenzene radicals, namely α, β, γ, and δ-butylbenzene radicals (eq 2). The abstraction of hydrogen on the ring is difficult since the phenyl C-H bond has a very high BDE (Table 3). Each of butylbenzene radicals could decompose by β-scission to form a small radical and an 1-alkene (eqs 3-6). These small radicals could, in turn, abstract hydrogen atoms from *n*-butylbenzene to produce the above four butylbenzene radicals and, thus, propagate the chain. The termination could occur by the recombination of any pair of radicals, as shown in eq 7.

The formation of toluene, styrene, ethylbenzene, and allylbenzene could easily be explained by the above primary reactions. Tetralin could be produced by the cyclization of a δ-butylbenzene radical. Benzene, in principle, could be formed from β-scission of a β-butylbenzene radical at the C_{ring}–C_α bond. Examination of BDEs in Table 3 reveals that the β-scission at the C_{ring}–C_α bond is unfavorable as compared to that at the C_γ–C_δ bond because of the much higher bond strength of the C_{ring}–C_α bond than that of the C_γ–C_δ bond. Freund and Olmstead [4] suggested that benzene is produced by "ipso" attack of hydrogen atoms on *n*-butylbenzene, eliminating substituted butyl radical and forming benzene. The hydrogen atoms needed for this reaction could be produced from β-scission of β-butylbenzene radicals at the benzyl C–H bond. This route for hydrogen production

seems reasonable because of the lower bond strength of the benzyl C–H bond than that of the C_γ–C_δ bond.

The significant formation of secondary products reveals that the following addition reactions occur:

$$C_6H_5CH{=}CH_2 + CH_3\cdot \rightarrow C_6H_5\dot{C}HCH_2CH_3 \quad (8)$$

$$C_6H_5CH{=}CH_2 + CH_3\cdot \rightarrow C_6H_5CH(CH_3)CH_2\cdot \quad (9)$$

$$C_6H_5CH{=}CH_2 + CH_3CH_2\cdot \rightarrow C_6H_5CH(CH_2CH_3)CH_2\cdot \quad (10)$$

$$C_6H_5CH_2\cdot + CH_2{=}CHCH_3 \rightarrow C_6H_5CH_2CH(CH_3)CH_2\cdot \quad (11)$$

$$C_6H_5\dot{C}HCH_2CH_2CH_3 + CH_2{=}CHCH_3 \rightarrow C_6H_5CH(C_3H_7)CH_2\dot{C}HCH_3 \quad (12)$$

$$C_6H_5CH{=}CH_2 + C_6H_5CH_2\cdot \rightarrow C_6H_5\dot{C}HCH_2CH_2C_6H_5 \quad (13)$$

$$C_6H_5CH{=}CH_2 + C_6H_5CH_2CH_2\cdot \rightarrow C_6H_5\dot{C}HCH_2CH_2CH_2C_6H_5 \quad (14)$$

$$C_6H_5\dot{C}HCH_2CH_2CH_3 + C_6H_5CH{=}CH_2 \rightarrow C_6H_5CH(C_3H_7)CH_2\dot{C}HC_6H_5 \quad (15)$$

The methyl radical could add to styrene to form either $C_6H_5\dot{C}HCH_2CH_3$ or $C_6H_5CH(CH_3)CH_2\cdot$ radicals, as shown in eqs 8 and 9. These two radicals would abstract hydrogen atoms from the surrounding reactant molecules to form *n*-propylbenzene and isopropylbenzene. Since the formation of a secondary benzyl radical is much easier than that of a primary radical, the yield of *n*-propylbenzene would be much higher than that of isopropylbenzene. This is the case, as shown in Figures 11 and 13. The ethyl radical could add to styrene to form the $C_6H_5CH(CH_2CH_3)CH_2\cdot$ radical (eq 10) which abstracts hydrogen from *n*-butylbenzene to produce *sec*-butylbenzene. The addition of the benzyl radical to the central carbon of propylene could produce the $C_6H_5CH_2CH(CH_3)CH_2\cdot$ radical (eq 11) which abstracts hydrogen from the reactant molecule to form isobutylbenzene. Isobutylbenzene could also be formed from the addition of a methyl radical to the allylbenzene at the central carbon of the side chain, followed by hydrogen abstraction. The addition of α-butylbenzene radical to the terminal carbon of propylene would produce $C_6H_5CH(C_3H_7)CH_2\dot{C}HCH_3$ (eq 12) which abstracts hydrogen from *n*-butylbenzene to form 1-propylbutylbenzene. The addition reactions between the benzyl radical and styrene and between the phenylethyl radical and styrene would produce $C_6H_5\dot{C}HCH_2CH_2C_6H_5$ (eq 13) and $C_6H_5\dot{C}HCH_2CH_2CH_2C_6H_5$ (eq 14), which could then be converted to 1,3-diphenylpropane and 1,4-diphenylbutane upon hydrogen abstraction. The formation of four C_6-diphenyls can be explained by the addition reactions between four butylbenzene radicals and styrene. For example, the addition of α-

butylbenzene radical to the terminal carbon of styrene would produce a radical as shown in eq 15 which, then, abstracts hydrogen from the reactant molecule to form 1,3-diphenylhexane.

The relative yields of the products depend on reaction conditions. At low loading ratios the major reaction products are from the primary reactions. Using the kinetic parameters given by Freund and Olmstead [4] for the thermal decomposition of *n*-butylbenzene, the relative rate constants for the formation of four butylbenzene radicals can be estimated. Assuming $CH_3CH_2\bullet$ as an attacking radical, at 425 °C the relative rates for the formation of α, β, γ, and δ-butylbenzene radicals would be 4.23:1.00:1.00:0.47, taking into account the number of abstractable hydrogen atoms. The relative formation rates of the four radicals are consistent with the relative stabilities of these radicals: secondary benzyl radical > secondary alkyl radical > primary alkyl radical. From this distribution of butylbenzene radicals one would expect higher styrene yield because of the higher concentration of the α-butylbenzene radicals. This is the case for the low pressures and low conversions, as shown in Figure 8. Also, one would expect the yield of allylbenzene and that of toluene to be roughly equal since the rates for the formation of the β and γ-butylbenzene radicals are the same. Examination of Figure 8 indicates that the yield of allylbenzene is much lower than that of toluene. This is due to the fact that the relative product yields depend not only on the relative formation rates of the butylbenzene radicals but also on the subsequent decomposition rates of these radicals.

According to the kinetic parameters suggested by Freund and Olmstead [4], the relative decomposition rates of α, β, γ, and δ-butylbenzene radicals are estimated to be 1:6:7300:13. It can be seen that the decomposition rate of the γ-butylbenzene radical is at least 10^3 times that of the β-butylbenzene radical. The extremely high decomposition rate of the γ-butylbenzene radical, as compared with those of other radicals, is due to the fact that the decomposition of the γ-butylbenzene radical results in the formation of the resonance-stabilized benzyl radical. This high decomposition rate of the γ-butylbenzene radical explains the high yield of toluene. Under the conditions used, the butylbenzene radicals would also participate in chain transfer reactions. Because of their lower decomposition rates, the α, β, and δ-butylbenzene radicals would have a higher probability of being involved in chain transfer reactions. As a result, the concentrations of the α, β, and δ-butylbenzene radicals participating in the decomposition reactions would decrease while that of the γ-butylbenzene radical would increase. As pressure increases, this difference in the decomposition steps would be more significant. This can be seen from Figure 8 which shows that as pressure increases, the yield of toluene (from the

decomposition of the γ-butylbenzene radical) increases while those of styrene (from the α-butylbenzene radical) and allylbenzene (from the β-butylbenzene radical) decrease.

At higher pressures the radical addition reactions become significant. As pressure increases, the yields of the secondary products would increase, as shown in Figure 9, because of the increased addition rate. The increasing importance of the addition reactions with the increasing pressure also contributes to the decreases in the yields of styrene and allylbenzene.

The formation of *n*-propylbenzene requires the migration of the methyl radical toward styrene. The methyl radical, together with allylbenzene, is formed from the β-scission of the β-butylbenzene radical. In the near-critical and supercritical regions, the methyl radical and allylbenzene would be surrounded by the dense *n*-butylbenzene molecules. Because of its high reactivity, the methyl radical could easily abstract a hydrogen atom from the surrounding *n*-butylbenzene to form methane, or, could react with allylbenzene (re-synthesis) to regenerate the β-butylbenzene radical or to form the $C_6H_5CH_2CH(CH_3)CH_2\bullet$ radical, before it can collide with styrene. As pressure increases, it would be more difficult for the methyl radical to encounter styrene because of the increased reaction rates between the methyl radical and *n*-butylbenzene/allylbenzene. This would result in a decrease in the yield of *n*-propylbenzene (also the yield of isopropylbenzene) and an increase in the yield of isobutylbenzene with the increasing pressure, as shown in Figure 9.

The radical addition reactions would be favored at lower temperatures because of the low activation energies. Therefore, for the similar conversions, the yields of styrene and allylbenzene would be lower and those of secondary products would be higher at lower temperatures, as shown in Figures 10 and 11.

Examination of Figure 12 reveals that the yield of ethylbenzene rapidly increases with the increasing conversion, indicating that ethylbenzene is not only a primary product but also a secondary product. The secondary ethylbenzene could be formed from the decomposition of high-molecular-weight compounds, and/or could be converted from styrene. The formation of ethylbenzene via styrene can be described by the addition of a hydrogen atom to styrene. followed by hydrogen abstraction. This reaction also contributes to the decrease in the yield of styrene.

References

1. Schobert, H. H.; Eser, S.; Song, C.; Hatcher, P. G.; Walsh, P. M.; Coleman, M. M. Advanced Thermally Stable Jet Fuels. Technical Progress Report (August 1992-October 1992), February 1993, The Pennsylvania State University.
2. Soave, G. Chem. Eng. Sci. 1972, 27, 1197-1203.
3. Benson, S. W. Thermochemical Kinetics. John Wiley & Son: New York, 1976.
4. Freund, H.; Olmstead, W. N. Int. J. Chem. Kinetics, 1989, 21, 561-574.

3. Thermal Degradation Studies of ^{13}C-labeled Dodecane Mixed with a Petroleum Derived Jet Fuel, JP-8P, Using Gas Chromatography-Select Ion Monitoring.
(Contributed by: Daniel E. McKinney, Jacqueline M. Bortiatynski, and Patrick G. Hatcher)

Introduction

Long chain *n*-alkanes in the carbon number range of C_7-C_{17} comprise approximately 70 vol. % of the commercial and millitary aviation jet fuels (1-3). Therefore, it is important to understand the thermal degradation mechanisms and kinetics of these saturated hydrocarbons in order to develop thermally stable fuels for future high-Mach aircraft which not only use the fuel for propulsion systems but also as a heat sink to cool the airframe, engine, and other system components. During this time the fuel may experience temperatures in the range of 400-500°C (4), and thus an important understanding of the pyrolysis mechanisms and rate of *n*-alkane degradation at these temperatures becomes important.

Site specific ^{13}C-labeling of hydrocarbons has been shown recently to be an excellent technique for following the rate of thermal degradation of specific target molecules in complex fossil fuel systems (5-7). This technique rivals that of model compound studies, since the calculated kinetic parameters and reaction mechanisms are based on experiments in which a target fuel component is thermally stressed in the presence of a complex fuel system. Burnham et al. (6) have developed an isotopic method in which a double-^{13}C label is detected by gas chromatography-mass spectrometry. In this method, *n*-alkanes derived from the thermal degradation of 1,2-^{13}C-hexadecane are monitored by plotting the ion chromatogram corresponding to m/z=31 which corresponds to the mass of the di-^{13}C-labeled fragment ion. However, caution must be exercised when applying this method due to error in the quantitation of the ion chromatograms.

McKinney et al. (5,7) have used primarily ^{13}C NMR techniques to follow the decompostion of singly ^{13}C-labeled hydrocarbons. In this methodology, reactions involving the ^{13}C-labeled carbon lead to significant changes in the chemical shift of this carbon in ^{13}C NMR spectra. By enriching the reactive compound with 100% ^{13}C at one reactive site, an enhancement in the ^{13}C NMR sensitivity is realized for the labeled carbon. Optimal results are only obtained with this method when the signals resulting from the ^{13}C-labeled carbons of the starting material and the products do not overlap with regions of the spectrum containing a large number of carbon signals. For example, a paraffin-rich mixture contains a large number of intense signals in the aliphatic region corresponding to methyl

and methylene carbons. A carbon-13 labeled aliphatic compound mixed with such a fuel at low concentration levels would not yield a discernable signal in this region.

In an effort to obtain quantitative data with a higher degree of certainty, over a large dynamic range, gas chromatography-select ion monitoring (GC-SIMs) and ^{13}C-labeling techniques have been used in model studies examining the thermal degradation of ^{13}C-labeled dodecane mixed with a petroleum-derived jet fuel, JP-8P. GC-SIMs is a GC-MS technique that is most often used for the precise quantification of trace level components. When combined, ^{13}C-labeling and GC-SIMs provides a quantitative method for monitoring the thermal degradation rates of specific molecules in fossil fuel systems. A petroleum-derived jet fuel, laced with 6-^{13}C-dodecane, has been thermally stressed at varying time and temperature regimes, and the product mixtures have been analyzed by gas chromatography (GC) and GC-SIMs in order to determine kinetic parameters for its thermal degradation.

Experimental

Reagent grade chemicals were purchased from Aldrich and isotopically enriched $K^{13}CN$ was purchased from Isotech Inc. 6-^{13}C-dodecane was synthesized using a similar reaction scheme as that described by McKinney et al. (7). The jet fuel sample used in this work is a petroleum derived JP-8 fuel with similar properties to those of commercial jet fuel Jet A-1 (Martel, 1987).

The synthesis of 6-^{13}C-dodecane was accomplished in a three-step synthetic pathway using a similar procedure as outlined by McKinney et al. (7). The resultant 6-^{13}C-dodecane (0.185 g) was thoroughly mixed with JP-8P (39.522 g).

Pyrolysis experiments for 6-^{13}C-dodecane in JP-8P were carried out in 15 mL stainless steal tubing bomb reactors (8). The sample (5 mL) was first purged with 6.9 MPa UHP N_2 (cold) in order to remove any dissolved oxygen within the sample, and subsequently repressurized with 0.69MPa UHP N_2. The samples were then heated in a fluidized sand bath for varying temperature and time regimes. After reaction of the sample was complete, the reactor was removed from the fluidized sand bath and quenched in a cool water bath. Only the liquid product was collected upon opening of the bomb and analyzed by gas chromatography (GC) and gas chromatography-select ion monitoring (GC-SIMs).

Quantitative gas chromatography was carried out on each sample using a Hewlett-Packard 5890 II Gas Chromatograph with flame ionization detection. The column used was a 30 m, 0.25 mm i.d., 0.25 μm film thickness, fused silica capillary column (J&W Scientific, Inc. DB-5). The internal standard was d_{26}-dodecane. Briefly, samples were prepared by mixing, in a 20 mL scintillation vial, approximately 30–50mg of thermally

stressed 6-^{13}C-dodecane-JP-8P mix, approximately 0.5 mg of internal standard, and 6.2 g of *n*-pentane. Approximately 1μL of the diluted sample was injected onto a split/splitless injector operating in the splitless mode and the column temperature was programmed from 40-240°C at a heating rate of 5°C/min.

Quantitative gas chromatography-select ion monitoring was carried out using a Kratos MS-80 RFA high-resolution gas chomatogram/mass spectrometer system. The diluted sample (1 μL) was injected onto a split/splitless injector operating in the splitless mode, and the column temperature was programmed from 40-135°C at a heating rate of 5°C/min and then ramped to 240°C at a heating rate of 15°C/min. The column used was the same type as used for GC analysis. Two ions were monitored during acquisition: *m/z* = 172.2035 and *m/z* = 197.52 corresponding to the M+1 parent ion peak of 6-^{13}C-dodecane and d_{26}-dodecane, respectively. Perfluorokerosene was used as a reference compound for the lock mass, *m/z* = 192.9888, which corrects for any drift in the magnetic field during acquisition. Data acquisition and analysis were accomplished using a Kratos DS90 system coupled to a Kratos Mach 3 system.

Quantitation of the GC-SIMs data for the 6-^{13}C-dodecane-JP-8P mixture was carried out using an internal standard method. First, unlabeled dodecane and d_{26}-dodecane were mixed in pentane at four varying concentration levels for the dodecane (25, 50, 75, and 150 ng/μL) while the d_{26}-dodecane concentration (50 ng/μL) remained constant in each of the four standards. Each of these samples was in turn analyzed using GC-SIMs analysis comparable to the same acquisition parameters as used for the thermally stressed jet fuel mixtures with one exception: the M+1 parent ion monitored for the unlabeled dodecane will be one mass unit less, *m/z* = 171.2035, than that monitored for the 6-^{13}C-dodecane. A plot of Area *n*-C_{12}/Area d_{26}-C_{12} versus Wt. *n*-C_{12}/Wt. d_{26}-C_{12} is depicted in Figure 14. As expected, the resultant curve is linear and described by the general formula y = mx + b where m is the slope and b is the xy-intercept:

$$\frac{\text{Area n-C}_{12}}{\text{Area d}_{26}\text{-C}_{12}} = 1.4623 \times 10^{-2} + 1.3671\left(\frac{\text{Wt. n-C}_{12}}{\text{Wt. d}_{26}\text{-C}_{12}}\right)$$

Rearranging this equation, one can determine the weight of *n*-C_{12} in the mixture, as determined by GC-SIMs, by knowing the area of *n*-C_{12}, the area of d_{26}-C_{12}, and the weight of d_{26}-C_{12}:

$$\text{Wt. n-C}_{12} = \frac{\left(\frac{\text{Area n-C}_{12}}{\text{Area d}_{26}\text{-C}_{12}} - 1.4623 \times 10^{-2}\right)}{1.3671} * \text{Wt. d}_{26}\text{-C}_{12}$$

It is assumed that the response of the M+1 parent ion detected for unlabeled dodecane, used to construct the calibration curve, is the same as the M+1 parent ion detected for the carbon-13 labeled dodecane.

Results and Discussion

In considering the thermal degradation of long chain *n*-alkanes, it has been shown that the rate is generally first-order in the reactant (9-12). These studies were all performed using model compounds in which the concentration of the starting *n*-alkane is relatively large at the beginning of the reaction in comparison to products. Thus, at low conversions, the rate of formation of products from the starting material is much, much larger in comparison to the reverse reaction in which the starting material is being formed by either recombination mechanisms of smaller chain *n*-alkanes or homolytic cleavage of C-C bonds in higher carbon chain *n*-alkanes. In general, it is assumed that in a model compound system at low conversions, one need not worry about the rate of formation of the model compound. This is not the case in complex fossil fuel systems, because the concentrations of these larger and smaller molecules, with respect to the target molecule, are significant. Thus, one must take into account the rate of formation as well as the rate of degradation of the target molecule.

Figure 15 displays a typical GC and GC-SIMs plot for the thermal degradation of 6-^{13}C-dodecane in JP-8P. Gas chromatography allows for quantifying all hydrocarbons in a complex fuel mixture. However, how does one differentiate between carbon-13 labeled dodecane and unlabeled dodecane present naturally in the fuel? As shown in Figure 15, GC-SIMs allows one to differentiate between hydrocarbons containing carbon-13's and those at natural abundance. This is done by monitoring the M+1 peak of the parent ion of the labeled compound. Since this ion corresponds to an M+2 peak of the unlabeled species, we do not expect to see any contribution from unlabeled species. Thus, one can discriminate between naturally occuring dodecane in the jet fuel and carbon-13 labeled dodecane added using GC-SIMs.

In considering the rate of degradation of 6-^{13}C-dodecane in JP-8P, it was stated earlier that one must also take into consideration the formation of dodecane from larger molecular weight *n*-alkanes and recombination of lower molecular weight *n*-alkanes.

However, statistically speaking, there is a low probability, in a diluted system, that an *n*-alkane having a carbon number greater than C_{12}, in the jet fuel range, will be carbon-13 labeled, and, thus degrade to form carbon-13 labeled dodecane. The same is true for a recombination mechanism of lower molecular weight *n*-alkanes in that the probability of a carbon-13 labeled dodecane being formed by recombination of a naturally abundant radical and a carbon-13 labeled one is insignificant. In this respect, one can observe the thermal degradation of carbon-13 labeled dodecane in a fossil fuel system without concern for the production of this species.

Figure 16 shows a stack plot of the gas chromatograms of 6-^{13}C-dodecane mixed in JP-8P at time 0, at 400°C for 6 hrs., at 431°C for 3 hrs., and at 470°C for 3 hrs. Conversion of 6-^{13}C-dodecane in JP-8P is denoted in the upper right hand corner of each chromatogram as determined by GC-SIMs. At this point, more data points are needed in order to calculate rate constants for the various temperatures used and to establish whether or not the reaction is first order with respect to 6-^{13}C-dodecane. Once this accomplished, the activation energy and preexponential factor can be calculated and compared to values obtained for the stressing of dodecane by itself.

Conclusions

Gas chromatography-select ion monitoring in combination with carbon-13 labeling has been demonstrated as an excellent technique for monitoring the thermal degradation of 6-^{13}C-dodecane in JP-8P. It was shown that, using this technique, one can discriminate between naturally occuring unlabeled dodecane in the system to carbon-13 added by differences in their molecular weights. Preliminary data have been shown for the conversion of 6-^{13}C-dodecane in JP-8P and future work will be done in order to determine the rates of thermal degradation, activation energy and preexponential factor. Also, future work will be done in order to demonstrate the applicability of this technique to other labeled hydrocarbons such as polycyclic aromatic hydrocarbons and alkylbenzenes.

References

1. Martel, C. R. *Military Jet Fuels 1944-1987*, Summary Report U. S. Air Force, AFWAL-TR-97-2062, **1987**, 662 pp.
2. Song, C.; Hatcher, P. G. *Prepr.-Am. Chem. Soc., Div. Pet. Chem. Prepr.*, **1992**, 37 (2), 529-539.
3. Lai, W.-C.; Song, C.; Schobert, H. H.; Arumugam, R. *Prepr.-Am. Chem. Soc., Div. Pet. Chem.* **1992**, 37 (4), 1671-1680.

4 Storch, D. M.; Harrison III, W. E. Fuels and Lubrication Division, U.S. Air Force Wright Laboratory, WPAFB, Personal communication, Nov 23, **1992.**

5. McKinney, D. E.; Bortiatynski, J. M.; Hatcher, P. G. *Energy Fuels* **1993**, (7), 578-581.

6. Burnham, A. K.; Gregg, H. R.; Braun, R. L. *Energy Fuels*, **1995**, (9), 190.

7 McKinney, D. E.; Bortiatynski, J. M.; Hatcher, P. G. *Prepr.-Am. Chem. Soc., Div. Pet. Chem. Prepr.*, **1996**, (), 534-538.

8. Song, C.; Eser, S.; Schobert, H. H.; Hatcher, P. G. *Energy Fuels*, **1993**, (7), 234-243.

9. Voge, H. H.; Good, G. M.; J. Am. Chem. Soc. **1949**, (71),593-597.

10. Fabuss, B. M.; Smith, J. O.;Lait, R. I.; Borsanyi, A. S.; Satterfield, C. N. *Ind. Eng.Process Des. Dev.* **1962**, (1), 293-299.

11. Fabuss, B. M.; Smith, J. O.; Satterfield, C. N. *Adv. Pet. Chem. Refin.* **1964**, (9), 158-201.

12. Zhou, P.; Crynes, B. L. *Ind. Eng. Che. Process Des. Dev.* **1986**, (25), 508-514.

Task 2 Investigation of Incipient Deposition

1. Deposit Growth During Heating of Coal-Derived Aviation Gas Turbine Fuels (Contributed by Prashant C. Sanghani and André L. Boehman)

In our previous report [1] we proposed a global kinetic scheme to describe the formation of deposits by direct deposition of radicals generated from tetradecane decomposition. We also mentioned that significant deposit growth occurs directly on the wall. The ultimate objective of this work is to describe the kinetics of deposit formation in sufficient detail and with sufficient accuracy from a complex mixture such as jet fuel. Development of a satisfactory kinetic model is essential for numerical simulation of complex reactive flows in aircraft fuel systems.

The global model proposed in a previous report [2] for deposit formation was:

$$F \xrightarrow{k_F} R \qquad \text{F = Tetradecane, R = Radical}$$

$$R + H_i \xrightarrow{k_{H_i}} \text{Stable Products} \qquad H_i = \text{Tetralins and Decalins}$$

$$R + D \xrightarrow{k_D} D \qquad \text{D = solids}$$

$$\frac{dR}{dt} = k_F F - R\sum k_{Hi} H_i - k_D R$$

$$\frac{dH_i}{dt} = -R\sum k_{Hi} H_i$$

$$\frac{dD}{dt} = k_D R$$

The values of the best fit parameters obtained were $k_F = 1.1 \times 10^{-4}$ s^{-1}, $k_{H.1} = 2.5 \times 10^{-4}$ $m^3/(kmol\ s)$, $k_{H.2} = 1.5 \times 10^{-4}$ $m^3/(kmol\ s)$, $k_D = 3.5 \times 10^{-8}$ m/s. It was possible to describe qualitatively the disappearance of tetradecane, hydrogen donors such as tetralins, decalins and growth of deposits. Here it was assumed that tetradecane undergoes decomposition

and forms radicals which are either stabilized by tetralins or decalins or react to form deposits.

With very low values of k_F it is possible to simulate the induction period observed experimentally, but it will produce such a low radical concentration that there will not be enough radicals left to form any solids at longer periods of stressing. Therefore it will not be possible to simulate the observed increase in the deposition rate at longer times. The challenge here is to incorporate enough information about the mechanisms of solid formation to enhance the quality of the model's predictions. This may require postulation of certain radical species that allow the induction period and the increase in deposition at longer times to be described mathematically. Unfortunately, our measurements of stressed fuel compositions do not yield information on radical concentrations. These must be inferred from assumed kinetic pathways.

Because of the problem mentioned above we are looking at the deposit formation reaction from a statistical view point. Some results have been reported recently [3]. It was reported earlier [4] that solids formation proceeds mainly through formation of alkylbenzenes as the important intermediate. But, during the pyrolysis of a mixtures of coal-derived jet fuel and tetradecane, it was observed that alkyl benzene concentration remains constant as shown in Fig. 17. Therefore, from a statistical viewpoint it can be concluded that alkylbenzenes do not play significant role under such circumstances. What we mean here is that in the previous work on tetradecane pyrolysis [4] deposit growth did not occur until significant amount of alkyl- benzenes appeared and therefore it was possible to conclude that alkylbenzenes are precursors of deposit formation. Alkylbenzenes also were found to produce significant amount of solids when they were pyrolyzed individually [6]. However, there have been numerous studies showing that compounds behave differently in mixtures than during neat pyrolysis [e.g., 7]. It was also reported earlier [5] that butadiene is an important precursor during coke formation reaction. No butadiene was detected in a our stressed fuel samples obtained at various reaction times. This does not necessarily mean that butadiene is not involved in solid formation process. It might be so reactive that it do not remain in the sample after the reaction.

It is also [5] mentioned in the literature that alkenes are a precursor for solid formation. Lower molecular weight alkenes such as butenes and pentenes coelute with *n*-alkanes and cycloalkanes. Because of this, we were not able to quantify alkenes with good confidence. We are working on the use of a different column to separate lower molecular weight alkanes, alkenes and cycloalkanes with good resolution.

The role of lower alkenes and butadiene is still under investigation. In the previous model [2] cycloalkanes such as C_1- and C_2-cyclohexanes were also included to explore

their possibility as being hydrogen donors. This introduces a few more parameters and requires the development of a code which can couple ODEs (ordinary differential equations) with an optimization routine. Some success has been obtained in this area and this work is ongoing. When this optimization scheme for kinetic parameters is complete, we will be able to examine the efficacy of various kinetic models. Also, we will use this code to combine our predictions of deposit formation with statistical analyses of decomposition products to develop a procedure for accurate prediction of jet fuel decomposition..

References

1. Schobert et al., Advanced Thermally Stable Jet Fuels, Technical Progress Report, October 95 - December 95, 92PC92104-TPR-14.
2. Schobert et al., Advanced Thermally Stable Jet Fuels, Technical Progress Report, January 94 - March 1994, 92PC92104-TPR-7.
3. Sanghani P. C. and Boehman A. L.; *Prepr.- Am. Chem. Soc., Div. Pet. Chem.* 1996, 41 (2), 529-533.
4. Song C., Lai W. C., and Schobert H. H.; Ind. Eng. Chem. Res. 1994, 33, 534-547.
5. Froment G. F.; Reviews in Chemical Engineering, 1990, vol. 6, No.4, 293-328.
6. Peng Y. Ph.D. Dissertation, Dept. of Materials Science & Engineering, PSU 1995.
7. McKinney, D. E., Bortiatynski J. M. and Hatcher P. G., *Prepr.- Am. Chem. Soc., Div. Pet. Chem.* 1996, 41 (2), 534-538.

2. Modeling Heat Transfer to Flowing Jet Fuels (Contributed by Mark A. Tercha and André L. Boehman)

Jet fuel flowing through fuel handling lines in aircraft is exposed to elevated wall temperatures and is heated. This process of heat exchange is controlled by molecular transport, convective transport and fuel properties. The result can be a substantial change in fuel composition due to thermal degradation, but the primary cause of these changes in fuel composition is heat transfer [1].

As part of our ongoing studies of advanced thermally stable fuels, we have begun numerical and experimental studies of fuel decomposition in flowing systems. Here we report preliminary results from calculations of heat transfer to a flowing fuel from heated stainless steel tubing. Comparison is made to experiments performed at Wright Laboratory, WPAFB and which were summarized, in part, in Ref. [2].

The basis for these calculations is the entry length heat and mass transfer model for flow in tubes, STANTUBE, developed by Kays and Crawford [3]. STANTUBE is a cylindrical coordinates version of the STAN5 boundary layer heat and mass transfer code. STANTUBE solves the governing equations for internal flows in cylindrical, axisymmetric tubes using finite differencing. It can consider developed, developing, laminar and turbulent flows. Turbulence is modeled by one of three means: (1) Prandtl mixing-length approximation; (2) a turbulent kinetic energy (TKE) scheme; or (3) an eddy diffusivity function. In the latter two models, the mixing-length approximation is used in the laminar sublayer region. STANTUBE is an interactive program which produces a complex summary output file. A second interactive program. TUBETRAN and subsequently, TUBETRA2, has been written to read and manipulate the output from STANTUBE so that particularly useful details can be extracted from the output file. These important features of the modeling calculations include: residence time distributions; mass distributions of times spent at particular temperatures; and depths of thermal penetration into fluid where temperatures that exceed those where decomposition reactions become greatly accelerated.

The results discussed here include a preliminary calculation and comparison to experimental data from Wright Laboratory. To obtain these numerical results, a new output file translation program, TUBETRA2, has been written and applied which reads in STANTUBE output and obtains mean temperature distributions and fluid temperature profiles. From the thermal and velocity profiles, residence times and times at particular temperatures will be calculated in subsequent work.

Measured tube wall temperature data serve as the wall temperature boundary condition for the STANTUBE solution. The experiments were performed on Norpar-13 flowing at 12 mL/min and 700 psig through 1/4" stainless steel tubing. Figure 18 presents the comparison of calculated mean fuel temperatures with both measured wall temperatures and mean temperatures calculated by J. Atria at Wright Laboratory. The Wright Laboratory calculations used variable fuel property data for n-dodecane from a NIST hydrocarbon property data base. The STANTUBE calculation used fixed property data based on the mean fluid temperature reached halfway through the heated tube. The STANTUBE prediction of T_{mean} compares well with the Wright Laboratory prediction, if one takes into account the difference in the handling of thermal properties. Near the entrance to the heated tube, the temperature dependent properties yield a Prandtl number of 8.9, while we have assumed 4.99 throughout the solution. Near the exit of the tube, temperature dependent properties give a value of 2.8 for Prandtl number. Correspondingly, STANTUBE predicts a lower mean fuel temperature near the inlet and a higher mean fuel temperature near the exit.

This comparison demonstrates our capability to calculate thermal transport to jet fuel in flowing systems. From these initial calculations we will begin building a flow reactor model for comparison to our flow reactor experiments and for formulation of kinetic models that describe pyrolytic jet fuel degradation in flowing systems.

1. Hazlett, R. N., Thermal Oxidation Stability of Aviation Turbine Fuels. ASTM Publication, Philadelphia, PA. 1991. pp.1-21.
2. Atria, J. V. and T. Edwards, "High Temperature Cracking and Deposition Behavior of an n-Alkane Mixture," *Prepr.- Am. Chem. Soc., Div. Pet. Chem.* 1996, 41 (2), 498-501.
3. Crawford, M.E. and W.M. Kays, STAN5 - a Program for Numerical Computation of Two-Dimensional Internal/External Boundary Layer Flows. Report No. HMT-23. Thermosciences Division, Department of Mechanical Engineering, Stanford University, Stanford, California. 1975.

Task 4. Coal-based Fuel Stabilization Studies

Towards the Design of Thermally Stable Jet Fuels at Both Moderate (<250°C) and High (>400°C) Temperatures. (Contributed by Maria Sobkowiak and Michael M. Coleman)

Having successfully discovered compounds that act as thermal stabilizers for hydrocarbon mixtures at temperatures in excess of 400°C [1,2], we are now confronted with a number of questions, the answers to which have important ramifications in the design, formulation and development of commercially viable high temperature stable jet fuels. Such fuels must also be stable (both thermally and oxidatively) at storage and moderately elevated temperatures (from ambient to say 250°C) which is in the autoxidative regime. Will the high temperature (>400°C) thermal stabilizers such as THQ, benzyl alcohol (BzOH) etc. also act as antioxidants at these lower temperatures? Will the fact that they are highly susceptble to oxidation lead to additional problems? Even if THQ and BzOH are inherently poor antioxidants at the lower temperatures, will the relatively high concentration (≈1–10 mole % compared to <500 ppm for a classic antioxidant) of the hydrogen donor offset this drawback? This represents the next real challenge, because classic antioxidants like the sterically hindered phenolics that operate well in the autoxidation regime actually *promote* free radical reactions in the pyrolysis regime. In other words, the additive introduced to prevent degradation of the fuel in storage and at moderately elevated temperatures can adversely affect the efficacy of the additive put in to retard the formation of carbonaceous solids at high temperatures (>400°C).

Previously, we showed that when mixtures of dodecane (Dod) with THQ and Jet A-1 fuel with both THQ and BzOH, are stressed at 250°C under air pressures of 100, 200, 300 and 400 psi for 1 hr, there are no large amounts of carbonaceous solids formed. These preliminary results were encouraging and we have continued to perform systematic experiments of the type described above at 250°C under an initial air pressure of 200 psi as a function of time. The object of these experiments is to formulate a jet fuel that will have enhanced thermal stability in both the autoxidative and pyrolysis regimes.

Samples of pure Dod or Jet A-1 and mixtures containing 5 vol % of THQ or BzOH based on Dod (or Jet A-1) were thermally stressed at 250°C under 200 psi air for 1, 2, 3 and 4 hrs using the method described in detail in the last report [3]. The results for Dod and Jet A-1 mixtures are summarized in Tables 4 and 5, respectively. As indicated in Table 4, in the Dod mixtures with THQ, there are no large amount of carbonaceous solids formed up to 4 hrs but the liquids are colored throughout and there is evidence of small amount of

oily smear on the walls of reactor, after 3 hours of stressing. The smear is soluble in acetone. The Dod/ BzOH mixtures stressed under the same conditions show the presence of oil and carbonaceous solids. BzOH is not miscible with Dod at ambient temperature and there is no or very little improvement in stability over neat Dod.

The analogous results for the neat Jet A-1 and mixtures with THQ and BzOH are given in Table 5. In the Jet A-1 fuel mixtures with both THQ and BzOH, there appears to be a significant improvement. While the liquid is colored, carbonaceous solid formation appears to be retarded in the comparision with neat Jet A-1 fuel.

Clasic antioxidants such as the sterically hindered phenolics operate well in the autoxidation regime (<250°C). Will the addition of such oxidant like 2,6-di-*tert*-butyl-*p*-hydroxytoluene (BHT) to THQ and BzOH further improve their performance at the lower temperature (<300°C)? To answer this question we conducted a series of experiments where samples of dodecane mixtures containing 5% vol of THQ and BzOH were compared to analogous ternary mixtures containing 200 ppm BHT. These mixtures were stressed at 250°C under air pressure of 100 psi for 1 hr. The results are shown in Table 6. The addition of 200 ppm BHT to the mixtures of Dod with THQ produce clear, less colored liquids as compared the binary mixture of Dod with THQ. In the case of mixture Dod with BzOH the difference is less pronouced, but this is probably due to the limited solubility of BzOH in Dod at ambient temperatures. These mixtures now need to be characterized to determine the major reactions that have occured and this work is in progress.

References

1. *High Temperature Stabilizers For Jet Fuels And Similar Hydrocarbon Mixtures.Comparative Studies Of Hydrogen Donors.* E. M. Yoon, L. Selvaraj, C. Song, J. B. Stallman and M. M. Coleman, *Energy & Fuels*, submitted.

2. *High Temperature Stabilizers For Jet Fuels And Similar Hydrocarbon Mixtures. Kinetic Studies.* E. M. Yoon, L. Selvaraj, S. Eser and M. M. Coleman, *Energy & Fuels*, submitted.

3. M.M.Coleman, L.Selvaraj, M.Sobkowiak, *Advanced Thermally Stable Jet Fuels* Technical Progress Report, 92PC92104-TPR-14, December, 1995

Task 5. Exploratory Studies on the Direct Conversion of Coal to High-Quality Jet Fuels.

1. Contribution of Mineral Matter to Low Temperature Liquefaction Mechanisms. (contributed by Shona Martin)

Introduction

During coal conversion, the coal undergoes structural changes through reactions between coal constituents and solvent species or through catalytic reactions accelerated by added catalysts or the inherent mineral components. To date, the exact role of much of the mineral matter in coals remains unclear [1-3]. Typical interactions of mineral constituents and their behaviour at high temperatures is summarised in Table 7 [4].

These mineral and inorganic species can act as catalysts or poisons during liquefaction depending on reaction conditions. For example, minerals could act physically to block access to pores or reaction sites. Conversely, the chemical roles of inorganics include clays which can act as cracking catalysts and the hydrogenation catalyst, pyrite. Catalytic activity, mainly attributed to pyrite, is well documented [2,5]. Removal of naturally occurring cations such as Na^+, Ca^{2+} and K^+ has been shown to enhance liquefaction conversions [2,6] and several authors have observed a favorable influence of demineralization on coal depolymerization. Shams et al. [7] reported that the treatment of coals with methanol and HCl removes virtually all of the calcium species, leading to retardation of the retrogressive reactions Ca was proposed to catalyse.

The aim of the work reported here was to evaluate the nature and distribution of coal mineral matter in both untreated and treated (demineralized) samples of Wyodak coal, and consider the influence of these compounds by assessing their possible catalytic effect. To date, a series of experiments has been undertaken to compare the effect of demineralization on coal conversion at low temperatures (*ca* 300–350 °C), where preliminary results indicated that conversions were comparable upon pretreatment.

Experimental

1. Demineralization Wyodak coal (DECS-8) , ≤60 mesh, was obtained from the Penn State Coal Sample Bank. Proximate and ultimate analyses are as follows [8]: volatile matter (32.4%), fixed carbon (29.3%), moisture (28.4%), ash (9.9%), on an as-received basis; 75.8% C, 5.2% H, 1.0% N, 0.5% S and 17.5% O on a dmmf basis.

Demineralisation was facilitated by successive acid treatments. The first stage was an HCl wash (10 mL per gram of coal) to remove any alkaline earths which would form insoluble fluorides at the HF wash stage This was stirred at 60° C for 1 hour, filtered and washed. In the second stage, a 40% HF solution (10 ml per gram of coal) was digested at 60° C for 1 hour. The final sample was thoroughly washed with distilled water to ensure removal of residual HF. The filtrate was tested with $AgNO_3$ to indicate the presence of any residual chloride ions.

2. ICP-AAS Both the untreated and demineralised samples were analysed by ICP-AAS to more clearly identify the mineralogical distribution changes upon acid treatments. Samples were ashed at 950° C and the ash dissolved using a lithium metaborate fusion technique. Solutions were then analysed using a Leeman Labs PS3000UV inductively coupled plasma spectrophotometer (ICP).

3. Liquefaction Experimental procedures for liquefaction in tubing bombs have been outlined previously [9]. The conversion of coal into soluble products and gases was calculated on the basis of recovered THF-insoluble residue and reported on a dmmf basis. Residues were further analysed by FTIR and ^{13}C NMR.

4. FTIR Fourier transform infrared (FTIR) spectra of the demineralised coal and liquefaction residues were recorded on a Digilab FTS-60 spectrometer by co-adding 400 scans at a resolution of 2 cm^{-1}. The samples were prepared as KBr discs; predried sample (3 mg) was mixed with KBr (300 mg). All spectra were baseline corrected.

Results and Discussion

ICP-AAS As summarised in Table 8, metal concentration was determined by ICP-AAS in the normal and demineralised Wyodak coal samples. Ash was determined as 8.94 wt%. Upon demineralisation, ash concentration fell to *ca* 0.37 wt%, with the corresponding metal concentrations as indicated. All values are expressed in weight percent on an ash basis with the exception of HTA, which is on an as-received basis.

Liquefaction Data Results for the reactions conducted at 350 °C, both in the presence and absence of solvent, are reported in Table 9. For purposes of initial comparison, these will be discussed with respect to data with untreated Wyodak coal [10]. It is clearly demonstrated that demineralization imparts no seriously detrimental effects on liquefaction under such conditions.

The overall conversions and liquid product distribution indicates that the most significant changes occur in the presence of solvent, both H-donor and non-donor. In the absence of solvent, conversion can be considered to be solely due to pyrolysis, i.e. there are no solvent dissolution or H donation contributions. Higher conversion is the result of increased gas yield rather than liquid yield and quality. This may be derived from two contributions. If the reduction in Fe concentration, as highlighted by ICP, also comprises pyrite, this would account for the decrease in liquid yield. Moreover, if the increased gas make is due to CO_2, removal of the mineral matter may be considered to promote more facile pyrolysis of –COOH versus $-COO^-M^+$.

Reaction in the presence of the non-donor solvent, 1-methylnaphthalene, results in increases in both gas and liquid yield relative to the no-solvent situation. With "normal" coal and 1-MN, the increase in liquid yield for the raw coal is 5.1%. Presumably this increase is the "extra" liquid dissolved out by the solvent. With demineralised coal and 1-MN, the increased liquid yield is 12.4%. Therefore, the solvent is undoubtedly better able to dissolve material from the demineralised coal. This suggests that there is improved access of the solvent to the coal interior upon removal of mineral species.

The best liquid conversion, defined by oil concentration as a fraction of the total liquid yield, occurs upon reaction with tetralin. This is not surprising because tetralin is an H-donor, thus any enhancement in tetralin conversion relative to 1-MN can be attributed to H donation. The increase in liquid yield for normal coal in tetralin, relative to 1-MN, is 7.4%; the increase for demineralised coal is 8.6% The difference in these numbers is within experimental error, ±3%, hence demineralisation has no effect on H transfer from tetralin and there is no mineral matter catalysis of H donation.

Table 10 summarises the results of liquefaction conducted under an inert N_2 atmosphere and those facilitated in H_2. No significant deviation in overall conversion or product distribution was observed, even in the presence of solvent.

There are similarities between the results presented here and those of other studies, not necessarily limited to demineralised samples. Tomic and Schobert [11] also observed solvent effects under mild liquefaction conditions of subbituminous coals; the addition of a solvent was observed to enhance conversion relative to the reaction with no solvent, similar to the results in Table 10. And if, indeed, pyrite concentration has been reduced, the results in Table 10 confirm those reported by Tomic and Schobert [11], Artok [12] and Huang [13] who similarly reported that utilization of $H_2(g)$ is ineffective without a good hydrogenation catalyst, as illustrated by the similarities in the comparitive H_2 and N_2 runs. Serio et al. [3] also reported enhanced conversion for low rank coals following

demineralization This raises questions as to possible contribution of mineral species to low temperature liquefaction mechanisms. Joseph [6] ascribed this phenomenon to cations inhibiting hydrogen transfer from donor solvent/gaseous hydrogen to free radicals, in effect promoting retrogressive reactions. Therefore, it could be that the absence of these species allows for better access to reactive sites in the coal interior. Further, cations bound to organic functional groups bridge coal macromolecules, preventing dissociation and lowering their solubility during liquefaction. Hence, their removal from the coal enhances the dissolution and depolymerisation of coal macromoecules.

FTIR Comparative FTIR spectra of the normal and demineralised coal and associated residues from reaction at 350 °C under H_2 are shown in Figures 19 and 20. The spectrum of the whole demineralised coal indicates the presence of most of the groups of interest in this study.

Hydroxyl groups at	3300-3600 cm^{-1}
Aromatics	3030 cm^{-1} and associated bands at 1450-1600 cm^{-1}
Aliphatics	2920, 2850 cm^{-1}
Carboxylic acids	1710-1760 cm-1
Conjugated Ketones	1715 cm-1
Esters	1712-1735 cm^{-1} (present as a shoulder on the C=O band)

After reaction under H_2 at 350° C, the most notable feature of the whole product spectrum is a decrease in hydroxyl concentration, in part attributed to a loss of H_2O. Further examination of the THF-insoluble residue from this experiment confirms the loss of OH functionality coupled with the disappearance of the ester shoulder. The FTIR spectrum of the THF-insoluble residue from the reaction conducted with tetralin displays somewhat contrasting features. The carboxyl stretching region is much broader; moreover, the ester shoulder is more pronounced and the carbonyl region is much more defined.

The FTIR spectra of the THF-extracted raw coal and the residues from the runs conducted at 350° C under N_2 demonstrated that under all conditions, i.e. both in the presence and absence of solvent, no marked changes were observed. The residue from these sets of experiments is currently undergoing further analysis by Py-GC-MS, to evaluate in more detail the fundamental differences in speciation resulting from non-catalytic treatment under different regimes.

Conclusions

As anticipated, relative to runs at 350° C with untreated coal, demineralisation affords higher overall conversions; this trend becomes more apparent when either an H-donor (tetralin) or non-donor (1-mn) solvent are used. Specifically, there is no evident mineral matter effect on solvent H donation. Thus, initial results between the two sets of data suggests that the reactions undergone at 350° C are not mineral matter catalyzed.

With respect to mineral matter identification, further ICP-AAS studies have been conducted, in association with CC-SEM and XRD determinations to identify the mineral phases and species contributing to possible low temperature hydrogenation mechanisms.

References

1. Maldonado-Hodar, F.J., Rivera-Utrilla, J., Mastral-Lamarca, A.M., Ferro-Garcia, M.A. Fuel **74**(6), 818 (1995) and references therein.
2. Mochida, I., Yufu, A., Sakanishi, K., Korai, Y. Fual **67**, 114 (1988)
3. Serio, M.A., Solomon, P.R., Kroo, E., Bassilakis, R., Malhotra, R., McMillen, D.
Am. Chem. Soc., Div, Fuel Chem., Prep. **35**(1), 61 (1990)
4. Speight, J.G. "The Chemistry and Technology of Coal" Dekker, 1994
5. Garcia, A.B., Schobert, H.H. Fuel **68**, 1613 (1989) and references therein.
6. Joseph, J.T., Forrai, T.R. Fuel **71**, 75 (1992)
7. Shams, K., Miller, R.L., Baldwin, R.M. Fuel **71**, 1015 (1992)
8. Penn State Coal Sample Bank and Database
9. S.C. Martin, H.H. Schobert Advanced Thermally Stable Jet Fuels, Technical Progress Report, 92PC92104-TPR-11, p74
10. C. Song, A.K. Saini, H.H. Schobert Energy and Fuels **8**, 301 (1994)
11. Tomic, J., Schobert, H.H. Energy and Fuels **10** 1996 (in press)
12. Artok, L., Schobert, H.H., Erbatur, O Fuel Proc. Tech. **37**, 221 (1994)
13. Huang, L. PhD. Dissertation Thesis, The Pennsylvania State University, 1995

2. Exploratory Studies on Coal liquids Upgrading using Mesoporous Molecular Sieve Catalysts: Low-Temperature Hydrogenation of Aromatics over Mesoporous Zeolite-Supported Noble Metal Catalysts. (Contributed by Madhusudan Reddy Kondam and Chunshan Song)

Introduction

As part of our on-going effort to develop advanced thermally stable jet fuels from coal-derived liquids and petroleum, here we report the work concerned with deep hydrogenation of aromatics in fuels at low temperatures using mesoporous zeolite-supported noble metal catalysts. A high aromatic content is associated with poor quality, giving a high smoke point and low thermal stability of jet fuels. Saturation of naphthalene and its derivatives not only reduces aromatic contents of jet fuels, but also generates decalins which show much higher thermal stability than long-chain alkanes in jet fuels at high temperature (1).

The Clean Air Act Amendments of 1990 and new regulations call for the production and use of more environmentally friendly transportation fuels with lower contents of sulfur and aromatics (2, 3). High aromatic content in fuels lowers the fuel quality and contributes significantly to the formation of environmentally harmful emissions (4, 5). Deep hydrogenation has become necessary for reducing aromatic contents of fuels to meet increasingly more stringent regulations, because of the facts that 1) decreasing aromatics reduces catalytic converter light-off time, improves the converter efficiency and decreases exhaust hydrocarbons and 2) decreasing fuel polyaromatics reduces light-duty exhaust nitrogen oxides and particulate material and heavy-duty exhaust hydrocarbons. nitrogen oxides, and particulate material (4).

Currently, conventional hydrotreating technology is adapted for aromatics saturation. Typical conventional catalysts for fuel hydroprocessing are sulfided Co-Mo and Ni-Mo supported on alumina. Some studies have shown that complete hydrogenation of aromatics is not possible owing to equilibrium limitations under typical hydrotreating conditions, and existing middle distillate hydrotreaters designed to reduce sulfur and nitrogen levels would lower the diesel aromatics only marginally (4, 5). However, such catalysts are active only at relatively high temperatures (e.g., >300°C). Because hydrogenation is exothermic, deep hydrogenation is favored at lower temperature. It is therefore natural to consider deep hydrogenation at low temperatures (e.g., ≤300°C), and the potential candidate catalysts for low-temperature hydrotreating include noble metals. One of the options to improve the hydrogenation activities of noble metal-supported catalysts is to choose the proper support.

Previous work in this laboratory has shown that zeolites, Y and mordenite, are good supports for the Pt and Pd catalysts to hydrogenate the naphthalene more selectively to the thermally stable t-decalin (6-10). Since zeolites Y and mordenite are microporous in nature, hydrogenation of polyaromatic hydrocarbons can not achieved. Novel zeolite MCM-41, which is a mesoporous zeolite with very high surface area with mild acidity (11,12), can be a good support. In previous reports we have presented the synthesis, characterization and preliminary catalytic evaluation for the hydrogenation, hydrocracking and alkylation of bulky aromatic hydrocarbons (6-10, 13-20).

The objective of the present work is to explore the potential of mesoporous zeolite as support of noble metal catalysts for deep hydrogenation of aromatics in jet fuel. We have synthesized mesoporous zeolites with MCM-41 type structure using three different aluminum sources (6,13,15). We are currently exploring their applications for catalytic fuel processing (16-20). In our preliminary work, Pt/MCM-41 catalysts containing 3 wt% Pt were prepared with the mesoporous zeolites synthesized using pseudo-boehmite, Al isopropoxide, and Al sulfate, and applied for hydrogenation of naphthalene at 200°C and that of phenanthrene at 300°C (16,17). The results showed that the sample made by using Al isopropoxide gives the best catalyst. In the present work, supported catalysts containing 2 wt% Pt or 2 wt% Pd were prepared using proton-form MCM-41 (synthesized using Al isopropoxide) as well as Al_2O_3 and TiO_2 as the support materials. Their performance for hydrogenation of naphthalene in *n*-tridecane at 200°C is reported here.

Experimental

Catalyst Preparation

The mesoporous zeolite with MCM-41 type structure was synthesized using aluminum isopropoxide as the Al source according to the procedure described elsewhere (15). Supported catalysts containing 2 wt% Pt or 2 wt% Pd were prepared using proton-form mesoporous MCM-41 zeolite as well as Al_2O_3 and TiO_2 as the support materials. Table 11 gives their properties. The Pt catalysts were prepared by impregnation from aqueous solution of hydrogen hexacholoroplatinate (IV) hydrate, $H_2PtCl_6xH_2O$ (Aldrich, 99.995% Pt, metal basis). The Pd catalysts were prepared by impregnation of $PdCl_2$ (Aldrich, 99.999% Pd, metal basis) dissolved in dilute hydrochloric acid (sufficient to form soluble $PdCl_4^{2-}$). In both cases, water was removed by rotary evaporation at about 60°C. The catalyst precursors were dried in an oven at 60°C over night, and then calcined in an electric furnace at 450°C for 4 h. The nominal metal concentration was kept at 2 wt% for both Pt and Pd catalysts. Metal reduction was done in situ during naphthalene hydrogenation tests.

Catalyst Evaluation

All the catalysts were tested at 200 °C for a given residence time in 25-mL stainless-steel micro autoclaves. The total volume of the system including the connecting tube between reactor and pressure gauge is about 30 mL. Typically, the reactor was charged with 1.0 g naphthalene (Aldrich, 99%), 4.0 g n-tridecane solvent, and 0.1 g catalyst. The charged reactor was flushed with H_2, then pressurized to 1000 psig (cold) to start the test. The reactor was mounted on a holder, immersed in a fluidized sand bath preheated to 200°C, and shaken vertically at 240 cycles/min. with a 1 cm stroke.

At the end of the test, the reactor was taken out of the sand bath, quenched in cold water, and then allowed to cool down in air to room temperature. The gaseous products were collected for analysis and then the reactor was opened. The contents of the reactor were washed with acetone onto a filter. Solution products were analyzed by GC-MS and GC-FID. The capillary columns were 30mx0.25mm DB-5 (J&W Scientific) for GC-MS and 30mx0.25mm DB-5 (Hewlett-Packard), for GC-FID and the oven temperature program for both GC instruments was 60-280 °C at 10 °C/min. GC and GC-MS indicate that cracking or isomerization of *n*-tridecane, if any, were negligible. The yields of products were determined by quantitative GC analysis using n-nonane as internal standard, and the conversion was determined by the amount of naphthalene recovered after the reaction.

Selected tests were conducted to examine the effect of pre-reduction. Pre-reduction was carried out at 200°C for 1 h under reaction conditions except that naphthalene was not present during the reduction stage. After the reduction, the reactor was cooled down to ambient temperature, vented and opened. The reactor was re-sealed after the addition of 1 g naphthalene, and re-pressurized to 1000 psig H_2 at room temperature. Hydrogenation over the pre-reduced catalysts was also conducted at 200°C for 0.5 h.

Results and Discussion

Table 12 shows the distribution of products from naphthalene hydrogenation over Pd and Pt catalysts at 200°C for 60 min. The main products from naphthalene hydrogenation were tetrahydronaphthalene (tetralin or THN), and *cis*- and *trans*-decahydronaphthalene (decalin or DeHN). Δ9,10-octalin was also detected as a minor product in many tests, which is an intermediate from tetralin to decalin. The selectivity to tetralin+decalin+octalin approaches to unity in all the runs, indicating that there were essentially no side reactions such as ring-opening cracking and ring-contraction isomerization under the conditions. Based on the present and previous results (6-10, 21), the reaction pathways can be represented by Scheme I.

Effect of Supports

For Pt catalysts on different supports, the yield of tetralin decreased in the order of alumina > titania > MCM-41, whereas the yields of *trans*- and *cis*-decalins increased in the order of alumina < titania < MCM-41. In the case of Pt/MCM-41, the intermediate product

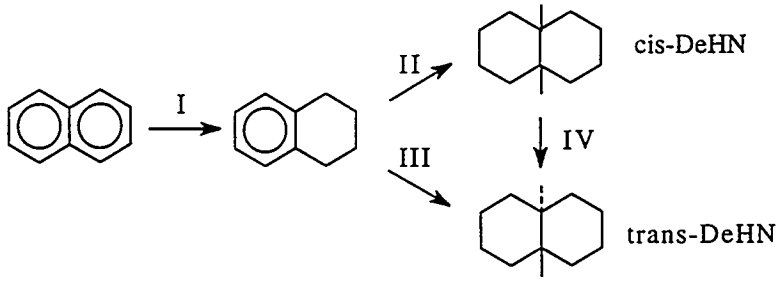

Scheme I

tetralin was almost completely hydrogenated, whereas tetralin still remains as a major product with Pt/Al_2O_3 and Pt/TiO_2.

For Pd catalysts; we observed essentially the same trends in terms of catalytic activity reflected by the increasing yields of decalins or decreasing yields of tetralin. Moreover, both Pd/MCM-41 and Pt/MCM-41 catalysts promoted the hydrogenation to completion such that the dominant products are *trans*- and *cis*-decalin, whereas tetralin is still one of the major products with both Al_2O_3- and TiO_2-supported Pd and Pt catalysts. These results indicate MCM-41 supported Pt and Pd catalysts are more active than titania and alumina supported catalysts.

The higher activity of the mesoporous zeolite-supported Pt and Pd may be due to better dispersion of the noble metals on MCM-41, since it has much larger surface than that of Al_2O_3 and TiO_2 supports (Table 11). According to a recent report (22), hydrogenation of naphthalene and benzene is insensitive to the geometric structure of the Pt species. The mild acidity of MCM-41 may also be a contributing factor, since it contributes to the electron deficiency of the metal on zeolite surface. It is known that noble metals on Y-zeolite and mordenite are often better dispersed and electron deficient as compared to those on alumina (4,5). The zeolitic protons can act as chemical anchors for reduced noble metal particles (23). Secondly, the noble metal, especially Pt, supported on acidic sites showed an unusually high tolerance towards sulfur poisoning (24). This unusual behavior of noble metals on acidic sites is again related to the electron deficiency of the noble metal: During ion-exchange or impregnation the metal attached to acidic site, then the calcination and reduction will lead to the small clusters of metal. The small clusters of metal atoms close to the acid sites are electron deficient responsible for the superior properties.

The selectivity to decalin isomers depends on the support and metal type. Compared to Pd/Al_2O_3 and Pd/TiO_2 catalysts, Pd/MCM-41 catalyst afforded higher *trans/cis* ratio, indicating a higher selectivity to *trans*-decalin. There appears to be one major difference between Pt and Pd catalysts in selectivity: Pd shows higher selectivity to *trans*-decalin. Therefore, among the three supports, MCM-41 corresponds to higher *trans/cis* ratios. Among the two metals, Pd catalysts always afford higher *trans/cis* ratios. Overall, MCM-41 supported Pd catalyst display highest selectivity to trans-decalin.

Effect of Reaction Time

Since complete naphthalene conversion was reached in 1 h, we reduced the residence time and conducted 30 min. runs at 200°C. Table 13 shows the results. Although unreduced catalysts were used, nearly complete naphthalene conversion was achieved in all the runs within 30 min. However, the product distribution changed with residence time. Yields of tetralin increased and decalin yields decreased with decreasing residence time. It is also clear that the absolute yields of tetralin and decalins strongly depended on the type of support and metal.

Even with reduced residence time, the MCM-41 supported Pt and Pd catalysts are substantially more active than the corresponding catalysts supported on alumina and titania (Table 13). In general, the activity of both Pt and Pd catalysts for complete hydrogenation of naphthalene to decalin decreased in the following order with respect to the support type: MCM-41 > TiO_2 > Al_2O_3.

When compared to the 60 min. runs, the yields of tetralin were generally higher and decalin yields lower in 30 min. runs, particularly when Pt or Pd was supported on alumina or titania. The *trans/cis* ratios of the decalin isomers are lower in the 30 min. runs than in 60 min. runs, even in the case of Pt/MCM-41 where tetralin was completely converted to decalin within 30 min. These results are consistent with Scheme I and indicate that *cis*-decalin isomerizes into *trans*-decalin during the hydrogenation reaction over MCM-41 supported catalysts, being consistent with the previous results from this laboratory (17, 25). TPD of *n*-butylamine indicates that hydrogen MCM-41 is acidic, but its acidity is lower than that of hydrogen Y zeolite. It appears from comparative examination that the presence of Pd metal and acid sites facilitates both tetralin hydrogenation and *cis*-decalin isomerization into *trans*-decalin.

Effect of Pre-Reduction

The above results clearly indicate that both Pd and Pt catalysts supported on the mesoporous MCM-41 are superior over those supported on Al_2O_3 and TiO_2. It should be noted that there may be two contributing factors, since the calcined catalysts were applied without reduction pretreatment. First, the in situ generation of active metal particles by H_2

reduction may be slower in Al_2O_3- and TiO_2-supported Pt and Pd than in MCM-41 supported metals. Second, the reduced metal species on MCM-41 are more active than those on Al_2O_3 and TiO_2. To see if this is the case, we examined the effect of pre-reduction punder reaction conditions (hydrogenation over the pre-reduced catalysts at 200°C for 0.5 h).

However the results (Table 14) showed that even after pre-reduction, the MCM-41 supported Pt and Pd catalysts are considerably more active than the corresponding Al_2O_3- and TiO_2-supported Pt and Pd catalysts. Like in the case of in situ reduced experiments, there are no or very less amounts of intermediate products tetralin and octalin found over MCM-41 supported catalysts, which confirms the complete hydrogenation of naphthalene to decalins. Whereas Al_2O_3- and TiO_2-supported Pt and Pd catalysts were not active enough for complete hydrogenation. It clearly confirms that the differences in activities are not due to the incomplete reduction of metals. Because our previous results of XRD suggested that the zeolite-supported Pt and Pd catalysts were completely reduced after 60 min. or 30 min. under comparable conditions (17, 25). The superior activity of MCM-41 supported catalysts should be exclusively due to the nature of reduced metal, where high surface and mild acidity of mesoporous MCM-41 must leading to highly dispersed and very active metal clusters. Another observation was that though the conversion and the basic trend of selectivity are same on both in situ reduced and pre-reduced catalysts, pre-reduced catalysts are slightly more active as we noticed from the decalin/tetralin and *trans-/cis*-decalin ratios (Table 14). Our earlier reports were also clearly indicated that in situ reduction is leading to fairly active catalysts. However the hydrogenation is a very sensitive reaction towards product selectivities, there were some discrepancies in the results of repeated experiments.

Conclusions

Mesoporous MCM-41 zeolite that was synthesized by a proper method may be used as a very effective support for noble metal catalysts. For hydrogenation of naphthalene in *n*-tridecane at 200°C, both the Pt and Pd catalysts supported on MCM-41 zeolite are substantially more active than the corresponding catalysts supported on Al_2O_3 and TiO_2. In general, the activity of both Pt and Pd catalysts for complete hydrogenation of naphthalene to decalin decreased in the following order with respect to the support type: MCM-41 > TiO_2 > Al_2O_3.

Both Pd/MCM-41 and Pt/MCM-41 catalysts promoted the hydrogenation to completion such that the dominant products are *trans*- and *cis*-decalin, whereas tetralin is still one of the major products with both Al_2O_3- and TiO_2-supported Pd and Pt catalysts. In

general, Pd catalysts showed higher selectivity to *trans*-DeHN, whereas higher selectivity to *cis*-DeHN was displayed by Pt catalysts.

The selectivity to decalin isomers also depends on the support and metal type. Among the three supports, MCM-41 gives higher *trans/cis* ratio. Among the two metals, Pd affords higher *trans/cis* ratio. In other words, Pd catalysts showed higher selectivity to *trans*-decalin, whereas higher selectivity to *cis*-decalin was displayed by Pt catalysts.

References

1. Song, C., Eser, S., and Hatcher, P. G., *Energy & Fuels*, **7**, 234 (1993).

2. Lee, S. L., Wind, M. De, Desai, P. H., Johnson, C. C., and Mehmet, Y. Asim, *Fuel Reformulation*, May/June, 26 (1993).

3. Unzelman, G. H., *Fuel Reformulation*, May/June, 38 (1993).

4. Stanislaus, A. and Cooper, B. H., *Catal. Rev. - Sci. Eng.*, **36**, 75 (1994).

5. Copper, B. H., and Donis, B. L. B., *Appl. Catal. A: General*, **137**, 203 (1996).

6. Schmitz, A. D., Bowers, G., and Song, C., *Advanced Thermally Stable Jet Fuels*, Technical Progress Report, 92PC92104-TPR-9, p. 37.

7. Schmitz, A. D., and Song, C., *Advanced Thermally Stable Jet Fuels*, Technical Progress Report, 92PC92104-TPR-10, p. 66.

8. Schmitz, A. D., and Song, C., *Advanced Thermally Stable Jet Fuels*, Technical Progress Report, 92PC92104-TPR-11, p. 61.

10. Schmitz, A. D., Bowers, G., and Song, C., *J. Catal.*, Submitted for publication, 1996.

11. Beck, J. S., J. C. Vartuli, Roth, W. J., Leonowicz, M. E., Kresge, C. T., Schmitt, K. D., Chu, C. T. W., Olson, D. H., Sheppard, E. W., McCullen, S. B., Higgins, J. B.,and Schlenker, J. C., *J. Am. Chem. Soc.*, **114**, 10834(1992).

12. Kresge, C. T., Leonowicz, M. E., Roth, W. J., Vartuli, J. C.,and Beck, J. S., *Nature*, **359**, 710(1992).

13. Reddy, K. M., and Song, C., *Advanced Thermally Stable Jet Fuels*, Technical Progress Report, 92PC92104-TPR-12, p. 42.

14. Schmitz, A. D., and Song, C., *Advanced Thermally Stable Jet Fuels*, Technical Progress Report, 92PC92104-TPR-13, p. 56.

15. Reddy, K. M. and Song, C., *Catalysis Letters*, **36**, 103(1996).

16. Reddy, K. M., and Song, C., *Am. Chem. Soc. Div. Fuel Chem. Prepr.*, **40** (4), 1003(1995).

17. Reddy, K. M. and Song, C., *Catalysis Today*, 1996, in press.

18. Song, C., Lai, W. -C., Schmitz, A. D., and Reddy, K. M., *Am. Chem. Soc. Div. Fuel Chem. Prepr.*, **41** (1), 71(1996).

19. Reddy, K. M., and Song, C., *Am. Chem. Soc. Div. Petrol. Chem. Prepr.*, **41** (3-4), (1996), in press.

20. Song, C., and Reddy, K. M., *Am. Chem. Soc. Div. Petrol Chem. Prepr.*, **41** (3-4), (1996), in press.

21. Lai, W.-C. and Song, C., *Catalysis Today*, 1996, in press.
22. Koussathana, M., Vamvouka, D., Economou, H., and Verykios, X., *Appl. Catal.*, **77**, 283(1991).

23. Satchtler, W. M. H., and Zhang, Z., *Adv. Catal.*, **39**, 129(1993).

24. Dauns, H., Ernst, S., and Weitkamp, J., *Stud. Surf. Sci. Catal.*,, **28**, 787(1987).

25. Schmitz, A., Bowers, G., and Song, C., *Catalysis Today*, 1996, in press.

APPENDIX I

TABLES

Table 1. Contributions of Sub-Groups (I_j).

Sub-group	Index
I_1 (primary carbon)	4
I_2 (secondary carbon)	10
I_3 (tertiary carbon)	13
I_4 (quaternary carbon)	5
I_5 (ring structure)	
cyclopentyl	27
cyclohexyl	30
decalin	37
I_6 (correction for)	
cyclopentane	+4
n-C_5 and cyclohexane	+2
each additional primary methyl group attached to a naphthenic ring	+1
each additional 1,5 H repulsion[a]	-3
conformational effect[b]	

a the repulsions between the H atoms attached to the 1,5 C atoms in such compounds as 2,2,4-trimethylpentane (Benson, 1976, p. 31).

b the group indices are tabulated for the more stable one of the conformational isomers; the values of the less stable isomers are calculated from the rate constant ratio of the two isomers at 450 °C as follows:

$$\frac{k_{\text{less stable}}}{k_{\text{more stable}}} = \exp\left[-0.75\ \Delta H_{rx}/(RT)\right]$$

where ΔH_{rx} is the heat of isomerization reaction between the conformational isomers (*cis* and *trans*).

Table 2. Reactive Structure Indices at 450 °C in 23.2-mL Reactor.

Compounds	Group distribution						
	a_1*I_1	a_2*I_2	a_3*I_3	a_4*I_4	a_5*I_5	a_6*I_6	RSI
n-Alkanes							
n-pentane	8	30	0	0	0	2	40
n-hexane	8	40	0	0	0	0	48
n-heptane	8	50	0	0	0	0	58
n-octane	8	60	0	0	0	0	68
n-nonane	8	70	0	0	0	0	78
n-decane	8	80	0	0	0	0	88
n-undecane	8	90	0	0	0	0	98
n-dodecane	8	100	0	0	0	0	108
n-tetradecane	8	120	0	0	0	0	128
n-hexadecane	8	140	0	0	0	0	148
Branched Alkanes							
2,2,4-trimethylpentane	20	10	13	5	0	-3	45
2,2,5-trimethylhexane	20	20	13	5	0	0	58
3-methylundecane	12	80	13	0	0	0	105
2,2,4,6,6-pentamethylheptane	28	20	13	10	0	-6	65
Monocyclics							
cyclohexane	0	0	0	0	30	2	32
methylcyclohexane	4	0	0	0	30	1	35
ethylcyclohexane	4	10	0	0	30	0	44
n-propylcyclohexane	4	20	0	0	30	0	54
n-butylcyclohexane	4	30	0	0	30	0	64
n-hexylcyclohexane	4	50	0	0	30	0	84
n-octylcyclohexane	4	70	0	0	30	0	104
n-decylcyclohexane	4	90	0	0	30	0	124
isopropylcyclohexane	8	0	13	0	30	0	51
tert-butylcyclohexane	12	0	0	5	30	0	47
isobutylcyclohexane	8	10	13	0	30	0	61
cyclopentane	0	0	0	0	27	4	31
methylcyclopentane	4	0	0	0	27	1	32
Bicyclics							
dicyclohexyl	0	0	0	0	60	0	60
dicyclohexylethane	0	20	0	0	60	0	80
dicyclopentyl	0	0	0	0	54	0	54
Steric Isomers							
trans-1,2-dimethylcyclohexane	8	0	0	0	30	2	40
cis-1,3-dimethylcyclohexane	8	0	0	0	30	2	40
trans-1,4-dimethylcyclohexane	8	0	0	0	30	2	40
trans-decalin	0	0	0	0	37	0	37

Table 3. Bond Dissociation Energies for *n*-Butylbenzene (kcal/mol).

C–C bond		C–H bond	
C_6H_5–$CH_2CH_2CH_2CH_3$	97.2	H–$C_6H_4CH_2CH_2CH_2CH_3$	110.9
$C_6H_5CH_2$–$CH_2CH_2CH_3$	68.6	$C_6H_5CH(CH_2CH_2CH_3)$–H	81.6
$C_6H_5CH_2CH_2$–CH_2CH_3	81.5	$C_6H_5CH_2CH(CH_2CH_3)$–H	94.5
$C_6H_5CH_2CH_2CH_2$–CH_3	85.2	$C_6H_5CH_2CH_2CH_2CH_2$–H	98.1

Table 4. Description of the products of thermal stressing at 200psi @ 250°C.

Time	Dodecane (Dod) Mixtures		
h	Neat Dod	+ 5% THQ	+ 5% BzOH
1	Pale yellow liquid No solids	Yellow/orange liquid No solids	Pale yellow liquid Oily drop, no solids
2	Pale yellow liquid Trace solids	Orange/brown liquid No solids	Light yellow liquid Oily drops, no solids
3	Yellow liquid Trace solids	Dark yellow liquid Oily deposit, soluble in aceton	Yellow liquid Oil , black solids suspended in oily phase
4	Yellow liquid Black solids	Dark yellow liquid Oily deposit, soluble in acetone	Yellow liquid Oil, black solids

Table 5. Description of the products of thermal stressing at 200psi @ 250°C.

Time	Jet A-1 Mixtures		
hr	Neat Jet A-1	+ 5% THQ	+ 5% BzOH
1	Yellow liquid Black solids	Yellow/orange liquid No solids	Yellow liquid No solids
2	Yellow liquid Black solids	Orange liquid No solids	Dark yellow liquid No solids
3	Dark yellow liquid Significant black solids	Orange liquid Oily drops, trace solid	Dark yellow liquid Oil , black solids
4	Yellow liquid Significant black solids	Orange liquid Black solids	Dark yellow liquid Oil, black solids

Table 6. Description of the products of thermal stressing at 100 psi @ 250° for 1 hr.

Dodecane (Dod) mixture	
Neat dodecane	Clear liquid
	No solid
+200 ppm BHT	Clear liquid No solids
+5% BzOH	Yellow iquid Oily drops, no solids
+5% BzOH @ 200 ppm BHT	Clear, bright yellow liquid Oily drops, no solids
+5% THQ	Yellow/orange liquid No solids
+5% THQ @ 200 ppm BHT	Clear, yellow liquid No solids

Table 7. General Behaviour of Minerals at High Temperatures.

INORGANIC SPECIES	BEHAVIOUR ON HEATING
Clays	Loose structural OH groups with rearrangements of structure and release of H_2O.
Carbonates	Decompose with loss of CO_2; residual oxides fix some organic and pyritic S as sulphate.
Quartz	Possible reaction with iron oxides from pyrite.
Pyrite	In air burns to Fe_2O_3 and SO_2.
Metal Oxides	May react with silicates.
Metal carboxylates	Decompose.

Table 8. Spectrochemical Analysis of Normal and Demineralised Wyodak Coal Samples by ICP-AAS.

		Metal Concentration (wt%)				
Sample	Ash	Fe	Ca	Mg	Na	K
Normal	8.94	5.53	13.2	3.02	1.12	0.78
Demineralised	0.37	56.8	9.23	1.51	0.20	0.24

Table 9. Results of Non-Catalytic Liquefaction of Normal and Demineralised Wyodak Coal
at 350 °C for 30 min. Under 6.9 MPa H_2.

Pretreatment	Solvent	Product Distribution (% dmmf basis)				
		Gas	Oil	Asph	Preasph	% Conv.
-	-	3.3	2.1	2.6	4.5	12.5
demineralised	-	10.0	0.8	0.4	5.3	16.6
-	Tetralin	4.2	4.1	7.6	10.0	25.9
demineralised	"	12.0	7.1	6.3	14.4	40.3
-	1-MN	4.0	1.1	5.8	7.4	18.3
demineralised	"	7.7	5.6	3.3	10.3	26.9

Table 10. Results of Non-Catalytic Liquefaction of Demineralised Wyodak Coal at 350 °C for 30 min. Under 6.9 MPa H_2 and N_2.

Gas	Solvent	Product Distribution (% dmmf basis)				
		Gas	Oil	Asph	Preasph	% Conv.
H_2	-	10.0	0.8	0.4	5.3	16.6
N_2	-	10.7	1.2	0.7	5.2	17.8
H_2	Tetralin	12.0	7.1	6.3	14.4	40.3
N_2	"	10.4	10.3	3.6	17.8	42.1
H_2	1-MN	7.7	5.6	3.3	10.3	26.9
N_2	"	8.7	5.8	1.4	8.4	24.4

Table 11. Properties of the Mesoporous MCM-41 Zeolite, Titania and Alumina Supports

Support ID	Material Type	Surface Area, m^2/g	Pore Vol cc/g	SiO_2/Al_2O_3 mol ratio	Source
MCM-41	Mesoporous zeolite	1206	1.77	40.7	PSU Fuel Science, Synthesized with AI
TiO_2	Titania	53	---	---	Degussa, Titania P25
Al_2O_3	γ-Alumina	113	---	<0.001	Degussa, Aluminum Oxide C

Table 12. Hydrogenation of Naphthalene at 200°C for 60 min over Pt and Pd Catalysts

Expt ID	79	115	81	82	83	84
Catalyst	Pt/Al_2O_3	Pt/TiO_2	Pt/MCM-41	Pd/Al_2O_3	Pd/TiO_2	Pd/MCM-41
Conversion (%)	98.3	99.9	100.0	99.9	99.9	100.0
Selectivity (wt%)						
Tetralin	57.0	35.8	0.0	42.5	30.5	0.0
9,10-Octalin	0.8	1.0	0.0	0.7	0.3	0.0
trans-Decalin	10.6	14.9	50.2	34.6	43.9	64.4
cis-Decalin	31.1	47.9	49.4	22.0	25.1	35.4
Others	0.5	0.4	0.4	0.2	0.2	0.2
trans-/cis-DeHN	0.3	0.3	1.0	1.6	1.7	1.8
DeHN+Tetralin	98.7	98.6	99.6	99.1	99.5	99.8
DeHN/Tetralin	0.7	1.7	2444.3	1.3	2.3	1235.3

Table 13. Hydrogenation of Naphthalene at 200°C for 30 min over Pt and Pd Catalysts

Expt ID	109r	110	92	93	94	111r
Catalyst	Pt/Al_2O_3	Pt/TiO_2	Pt/MCM-41	Pd/Al_2O_3	Pd/TiO_2	Pd/MCM-41
Conversion (%)	97.2	99.9	100.0	99.9	100.0	99.9
Selectivity (wt%)						
Tetralin	68.9	51.9	0.1	81.3	62.6	17.1
9,10-Octalin	1.1	0.2	0.00	0.9	1.0	0.3
trans-Decalin	6.5	8.2	45.2	10.3	21.1	52.8
cis-Decalin	23.3	39.0	54.3	7.4	15.1	29.7
Others	0.2	0.7	0.6	0.1	0.2	0.1
trans-/cis-DeHN	0.3	0.2	0.8	1.4	1.4	1.8
DeHN+Tetralin	98.7	99.1	99.4	99.0	98.8	99.6
DeHN/Tetralin	0.4	0.9	2160.2	0.2	0.6	4.8

Table 14. Hydrogenation of Naphthalene at 200°C for 30 min over pre-reduced Pt and Pd Catalysts

Expt ID	117	100	119	102	121	104
Catalyst	Pt/Al_2O_3	Pt/TiO_2	Pt/MCM-41	Pd/Al_2O_3	Pd/TiO_2	Pd/MCM-41
Conversion (%)	99.5	99.8	100.0	100.0	100.0	99.9
Selectivity (wt%)						
Tetralin	50.1	34.0	0.1	61.3	50.2	1.3
9,10-Octalin	1.0	0.6	0.0	0.1	0.7	0.0
trans-Decalin	13.0	16.1	35.5	24.5	29.3	68.6
cis-Decalin	35.8	48.7	64.3	12.6	19.6	29.9
Others	0.1	0.6	0.1	1.5	0.2	0.2
trans-/cis-DeHN	0.4	0.3	0.6	1.9	1.5	2.3
DeHN+Tetralin	98.9	98.8	99.8	98.5	99.1	99.8
DeHN/Tetralin	1.0	1.9	1721.2	0.6	1.0	73.0

APPENDIX II

FIGURES

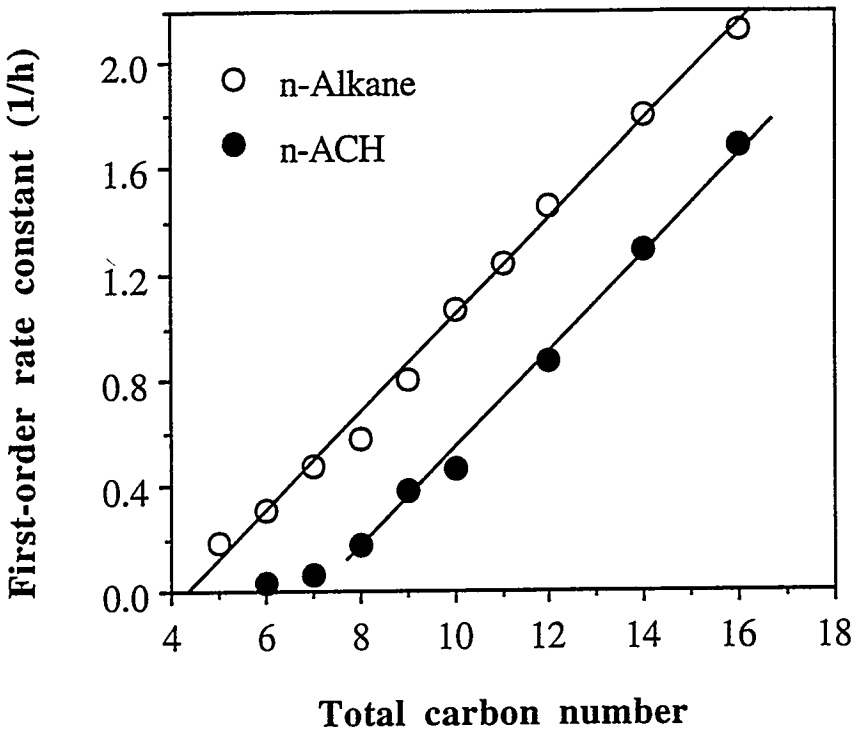

Figure 1. The Changes of Rate Constant with Total Carbon Number in Normal Alkanes and Normal Alkylated Cyclohexanes (*n*-ACH) at 450 °C in 23.2-mL Reactors.

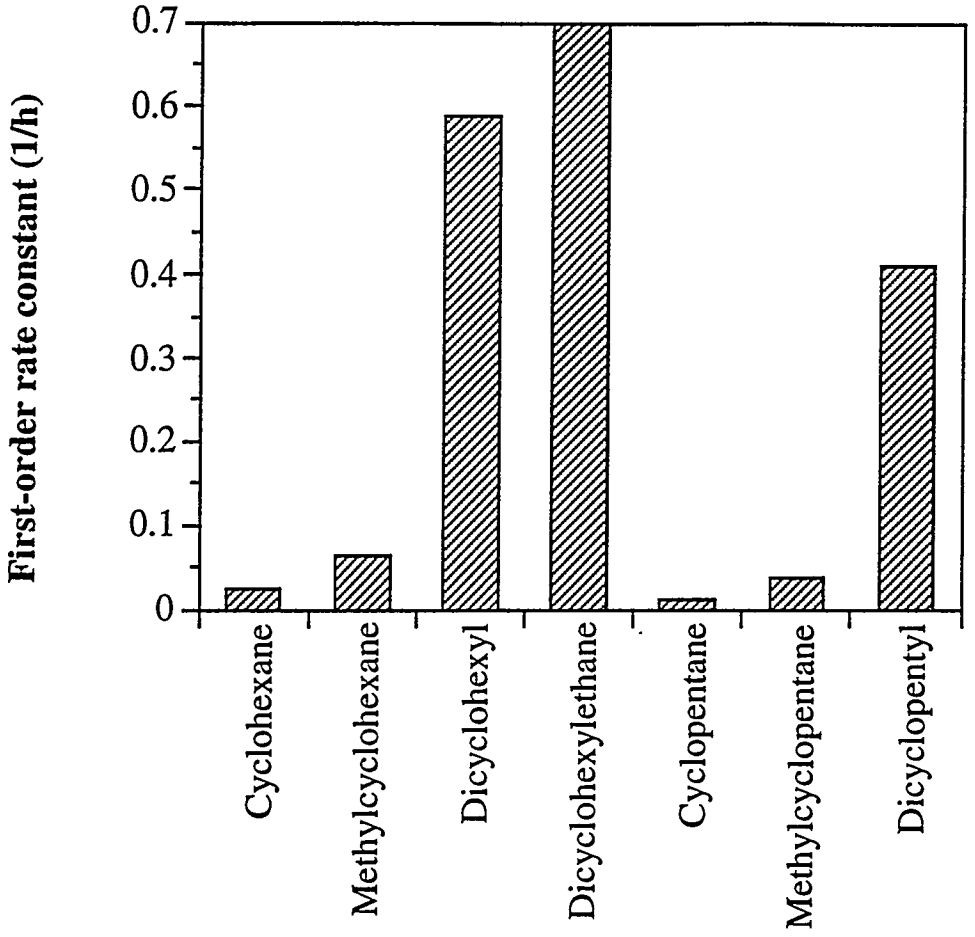

Figure 2. Rate Constants of Compounds with 5- or 6-Membered Ring at 450 °C in 23.2-mL Reactors.

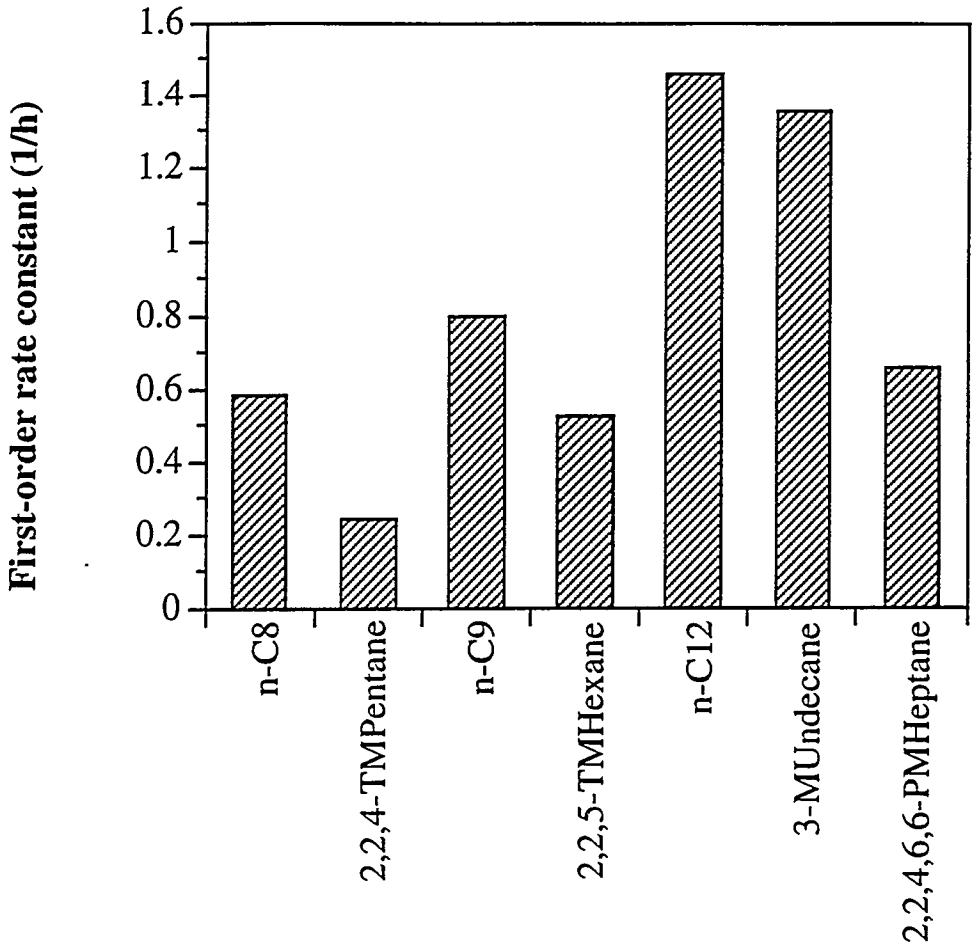

Figure 3. Rate Constants of Three Sets of Isomers (Normal and Branched Alkanes) at 450 °C in 23.2-mL Reactors.

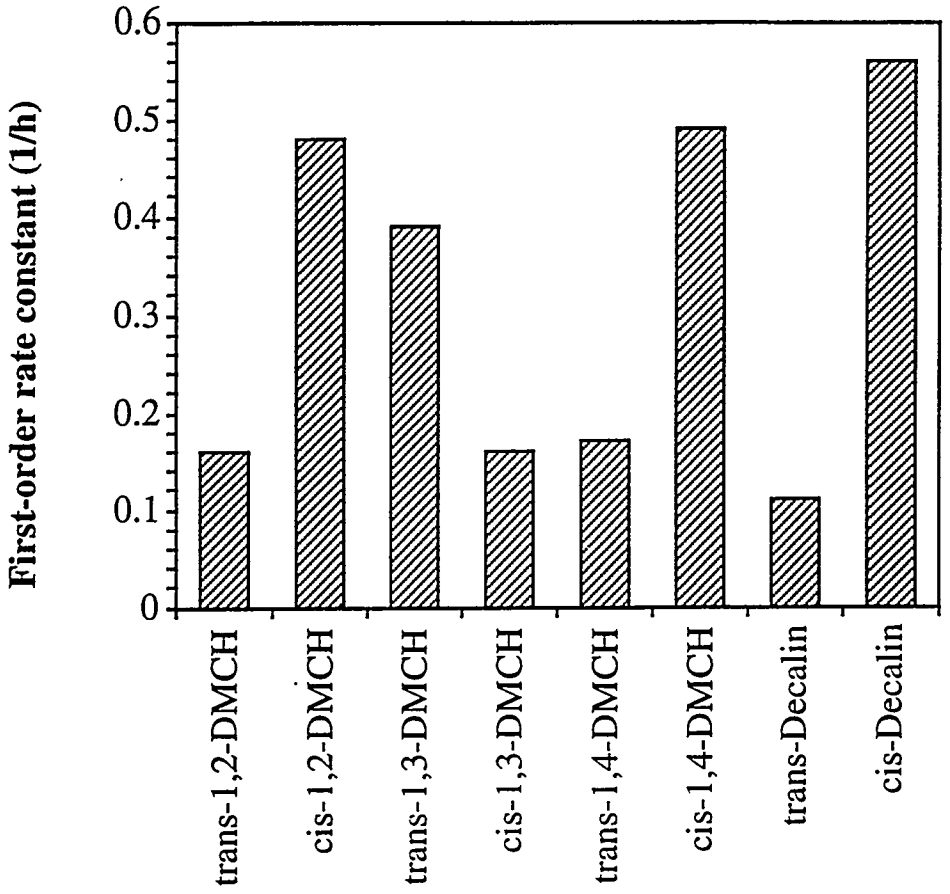

Figure 4. Rate Constants of Four Pairs of Steric Isomers at 450 °C in 23.2-mL Reactors.

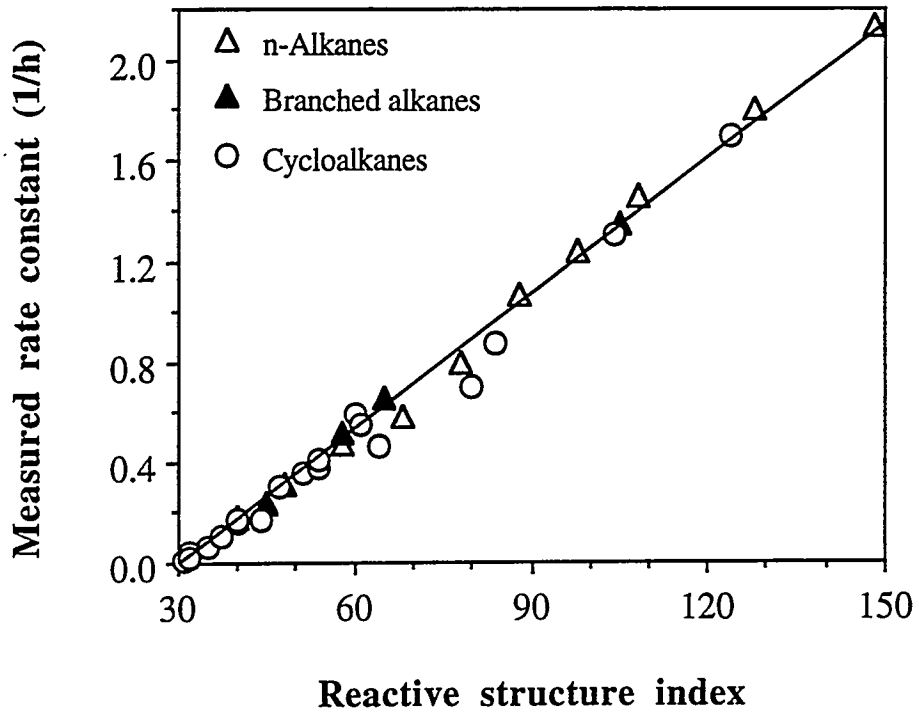

Figure 5. Experimental Rate Constants as a Function of Reactive Structure Index (RSI) at 450 °C in 23.2-mL Reactors.

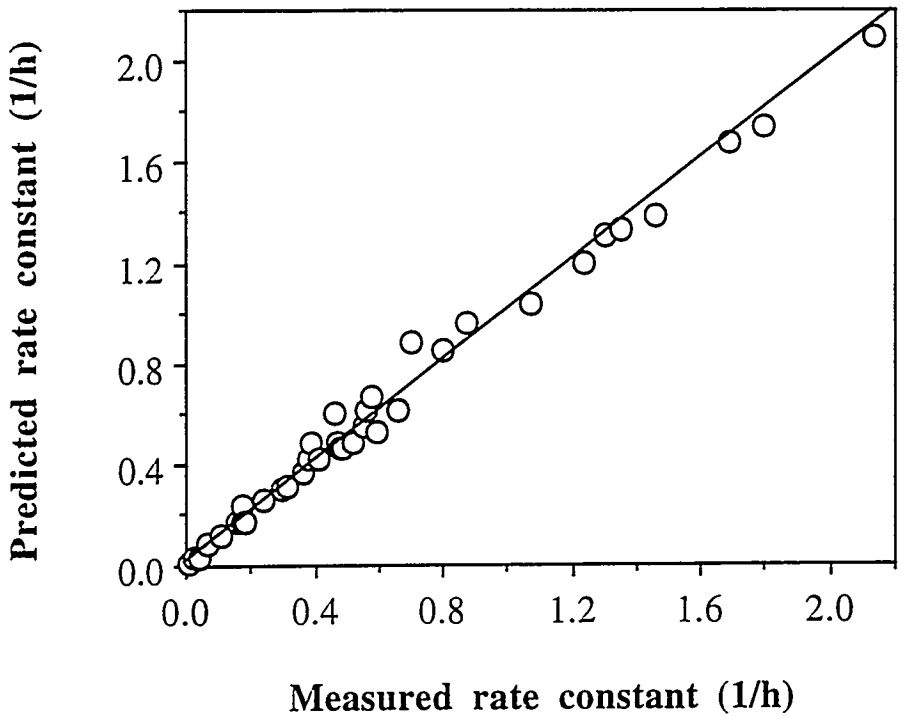

Figure 6. Predicted Rate Constants versus Experimental Values at 450 °C in 23.2-mL Reactors.

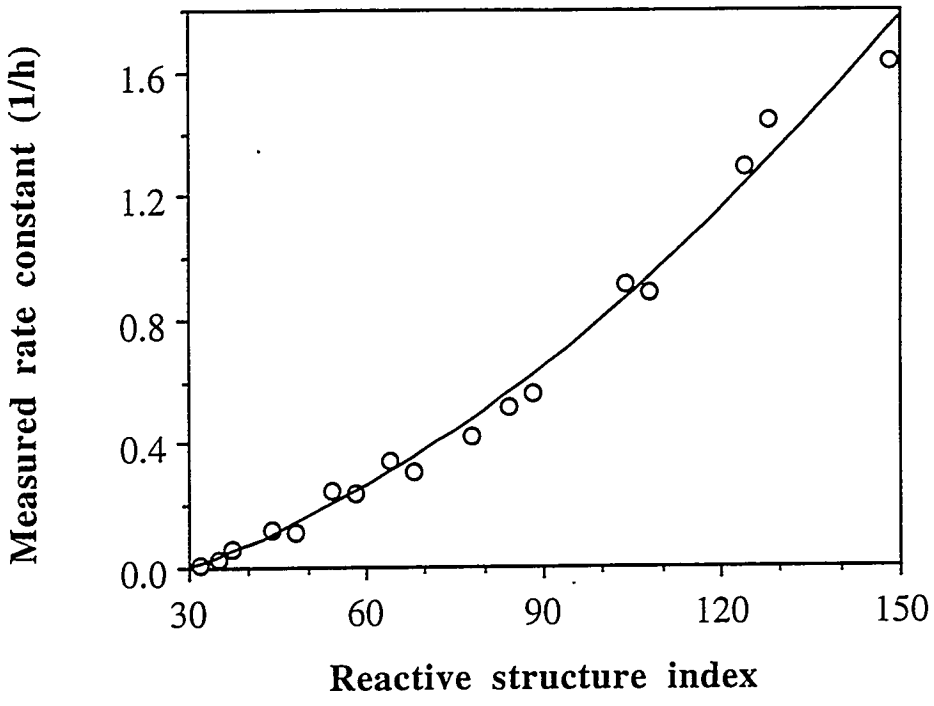

Figure 7. Experimental Rate Constants as a Function of Reactive Structure Index (RSI) in 28-mL Reactors.

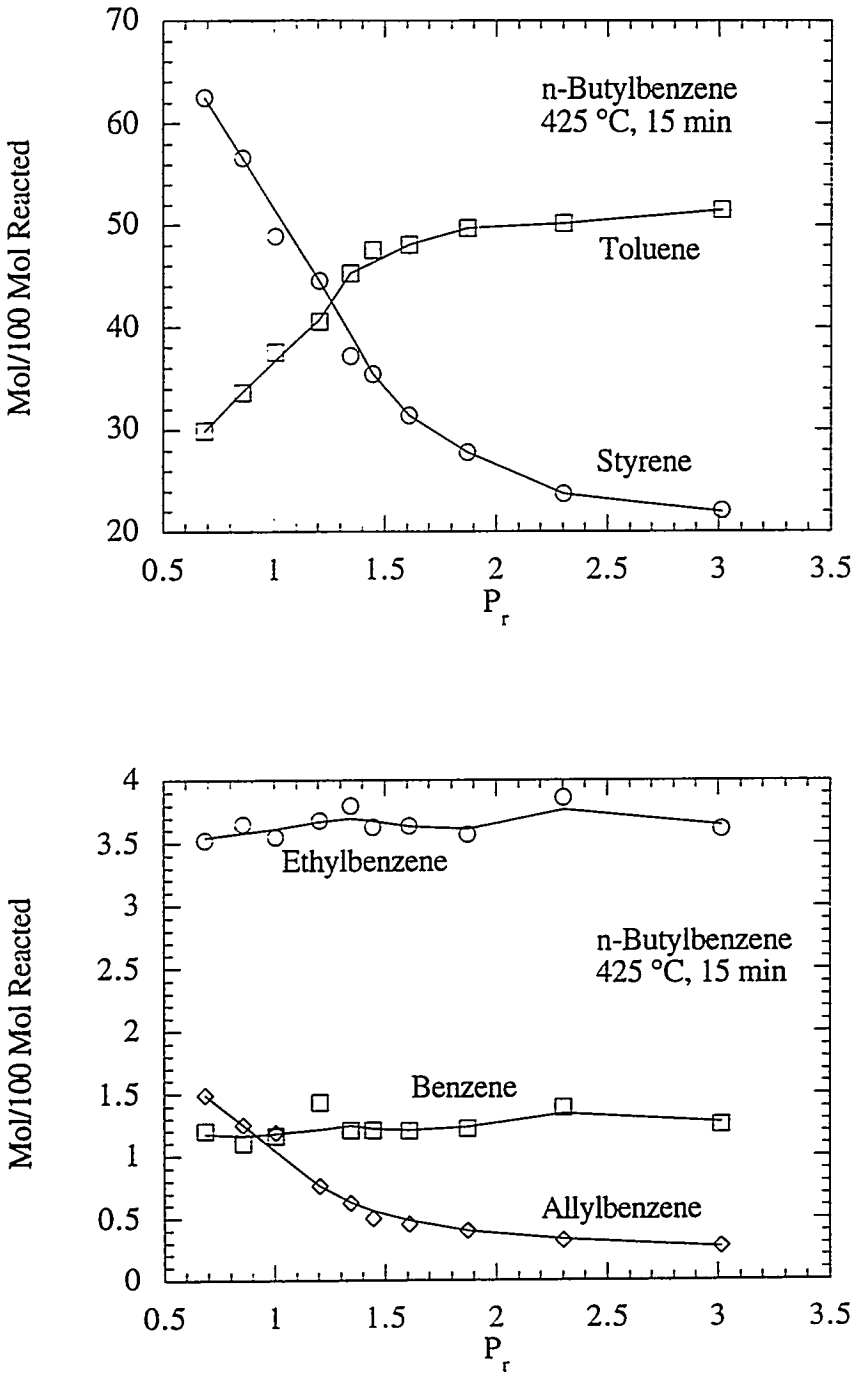

Figure 8. Primary Product Distributions as a Function of Initial Reduced Pressure for Thermal Decomposition of *n*-Butylbenzene.

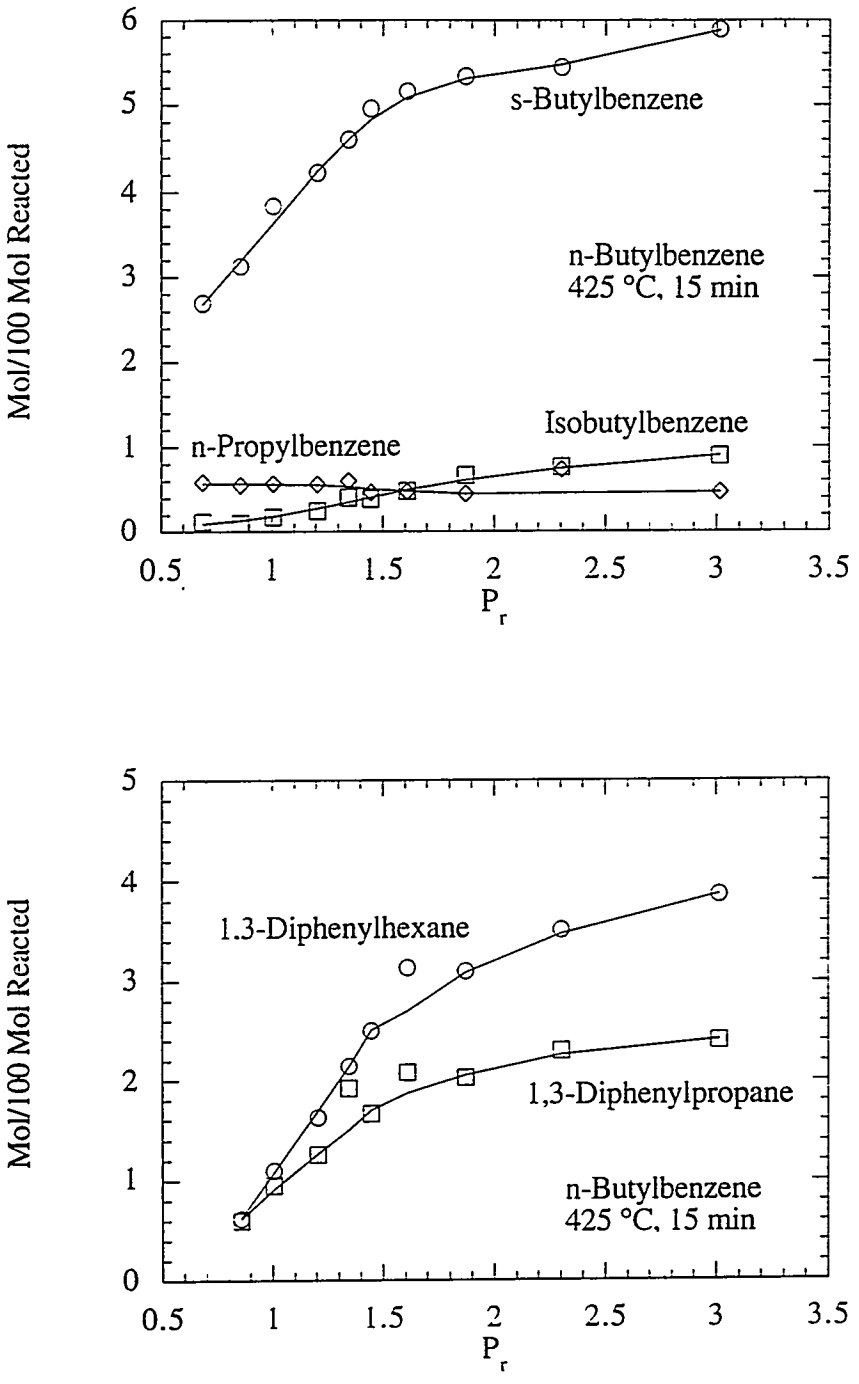

Figure 9. Secondary Product Distributions as a Function of Initial Reduced Pressure for Thermal Decomposition of *n*-Butylbenzene.

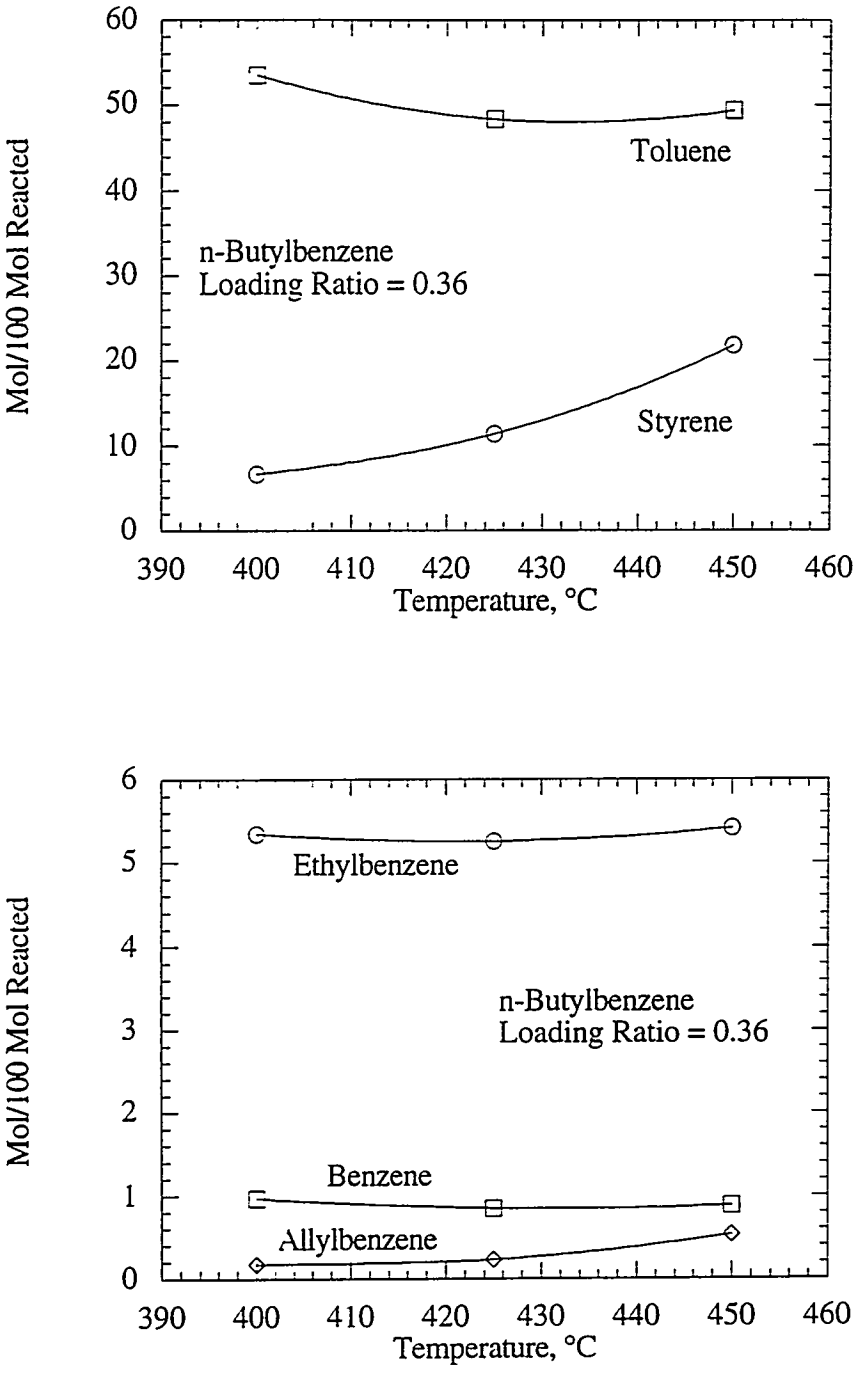

Figure 10. Primary Product Distributions as a Function of Temperature for Thermal Decomposition of *n*-Butylbenzene.

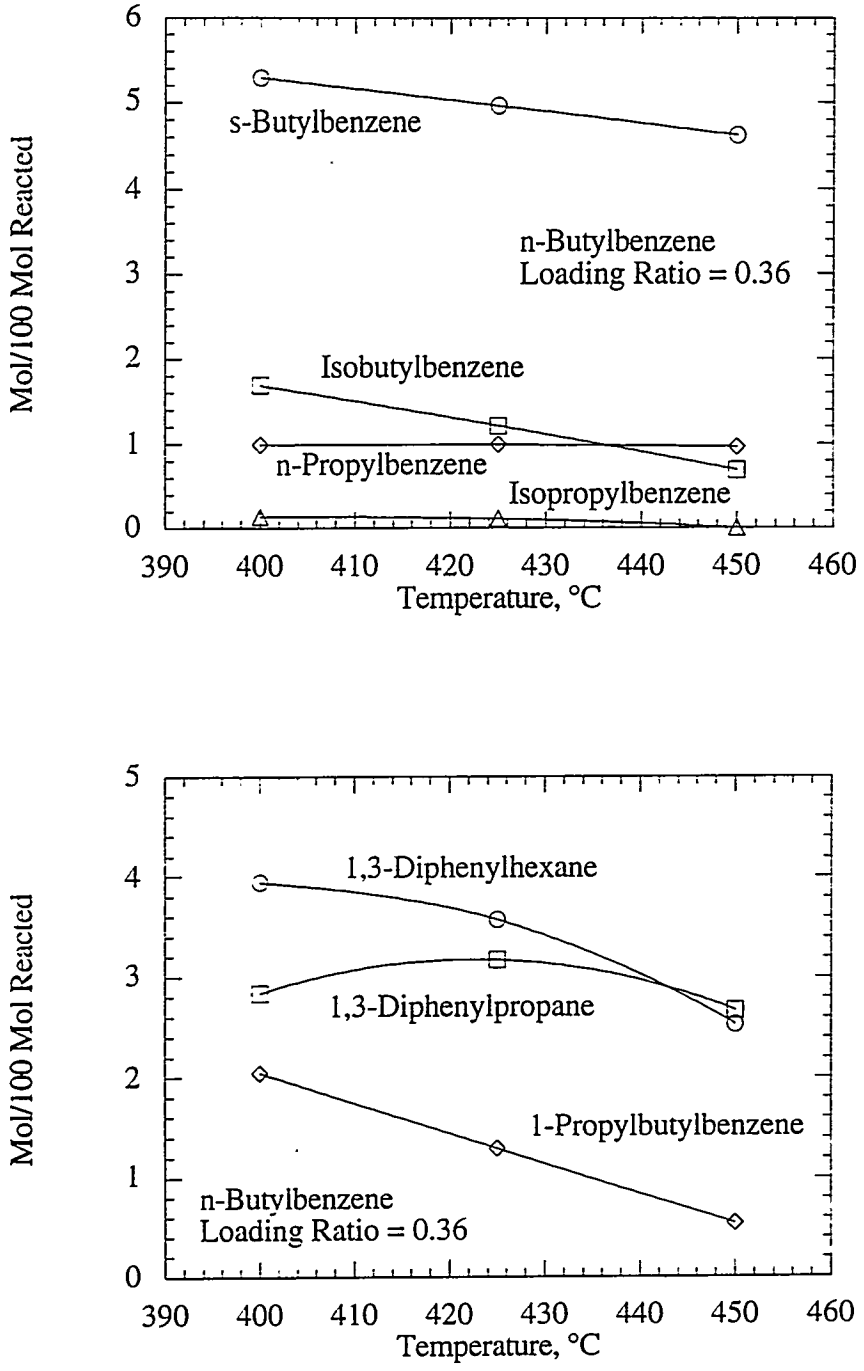

Figure 11. Secondary Product Distributions as a Function of Temperature for Thermal Decomposition of *n*-Butylbenzene.

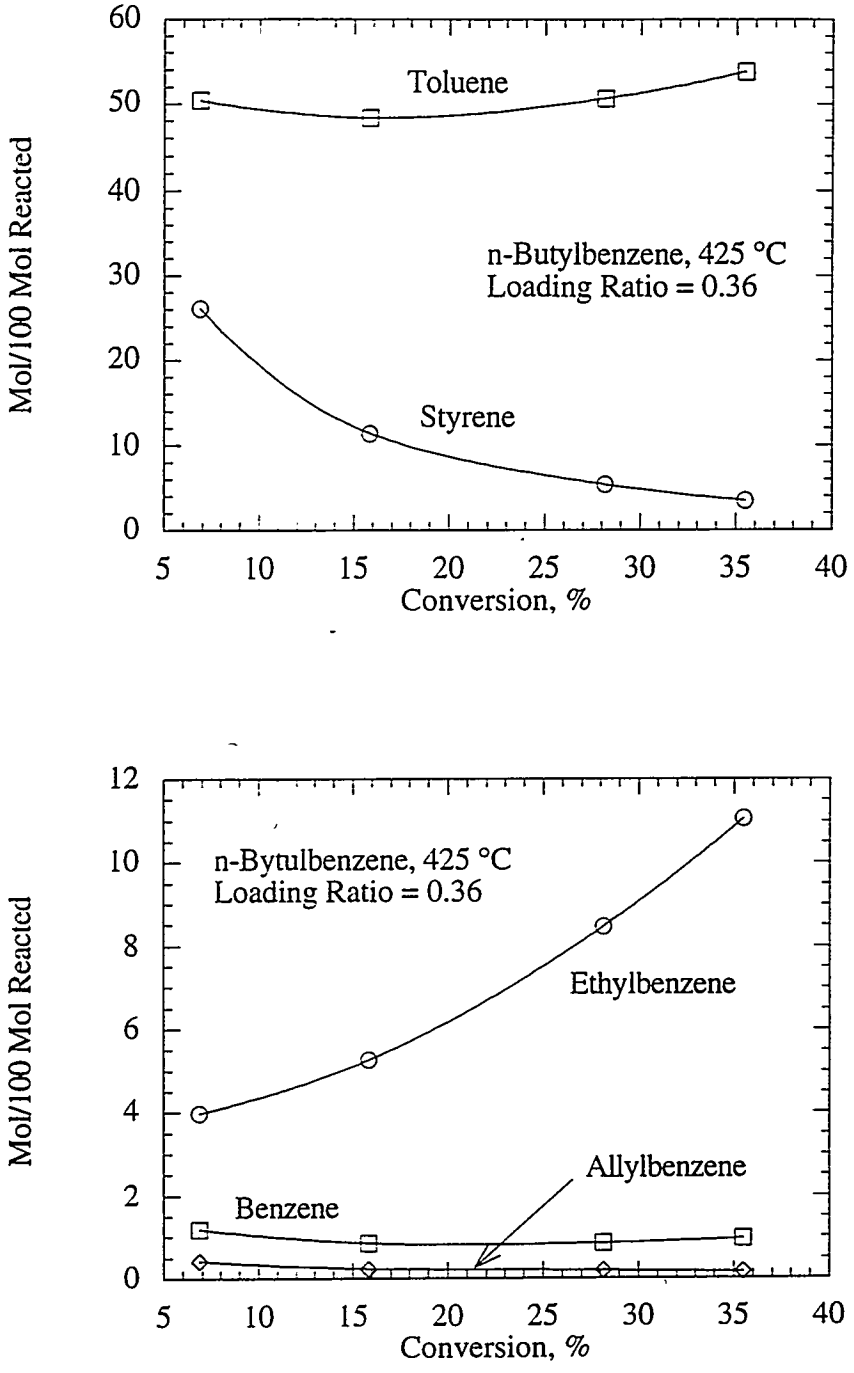

Figure 12. Primary Product Distributions as a Function of Conversion for Thermal Decomposition of *n*-Butylbenzene.

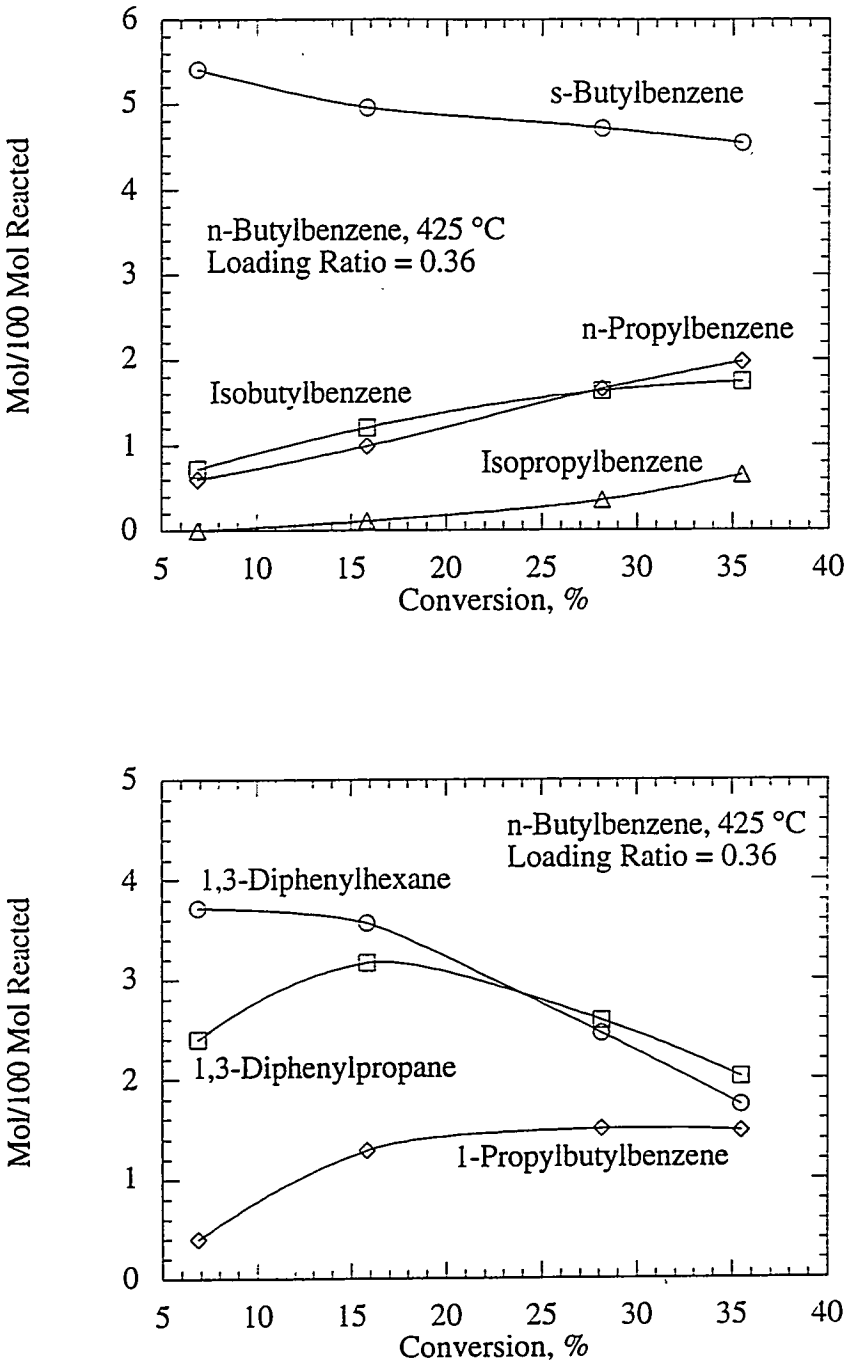

Figure 13. Secondary Product Distributions as a Function of Conversion for Thermal Decomposition of *n*-Butylbenzene.

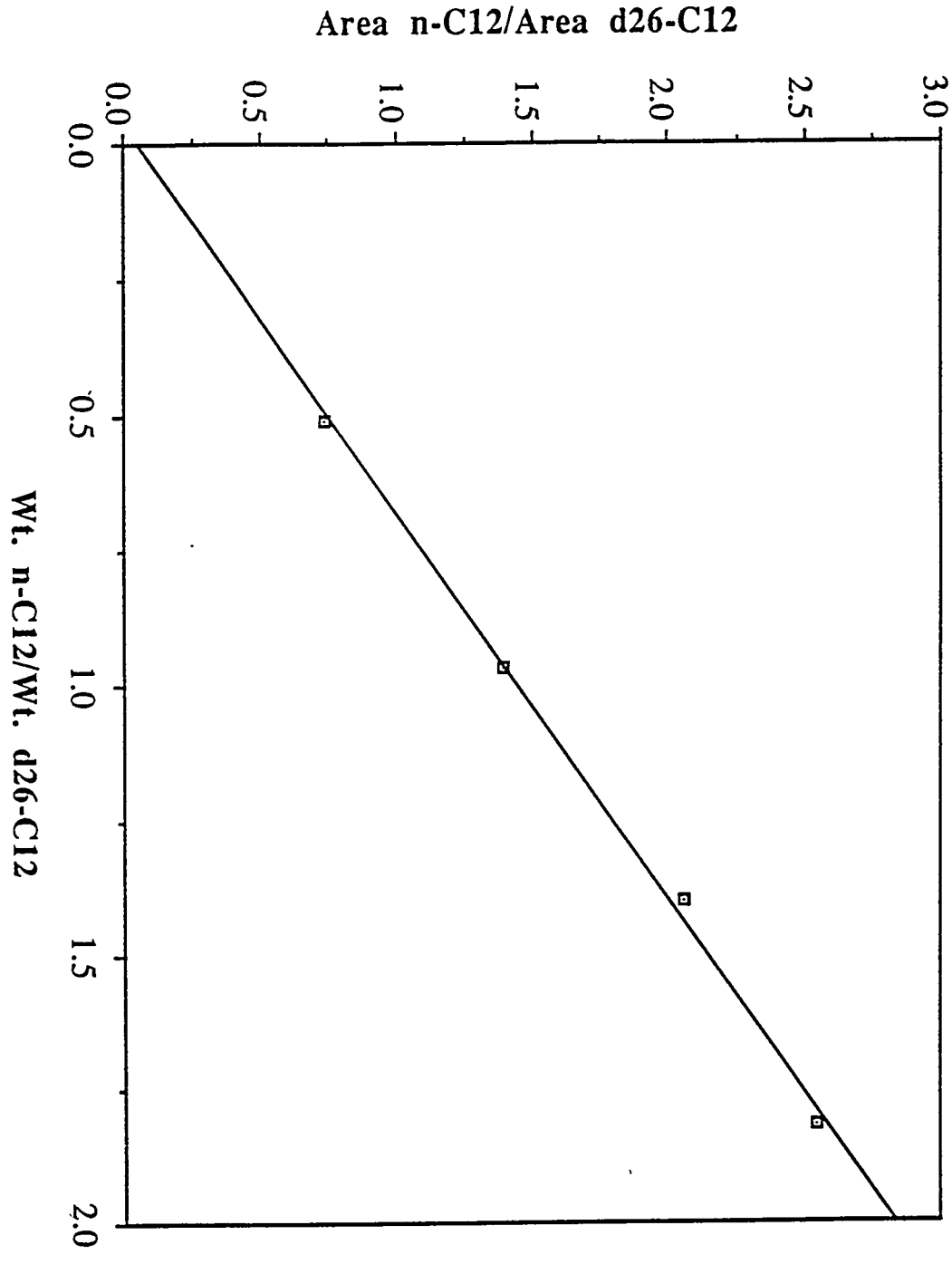

Figure 14: Plot of normalized area versus normalized weight for dodecane with respect to the internal standard, d_{26}-dodecane.

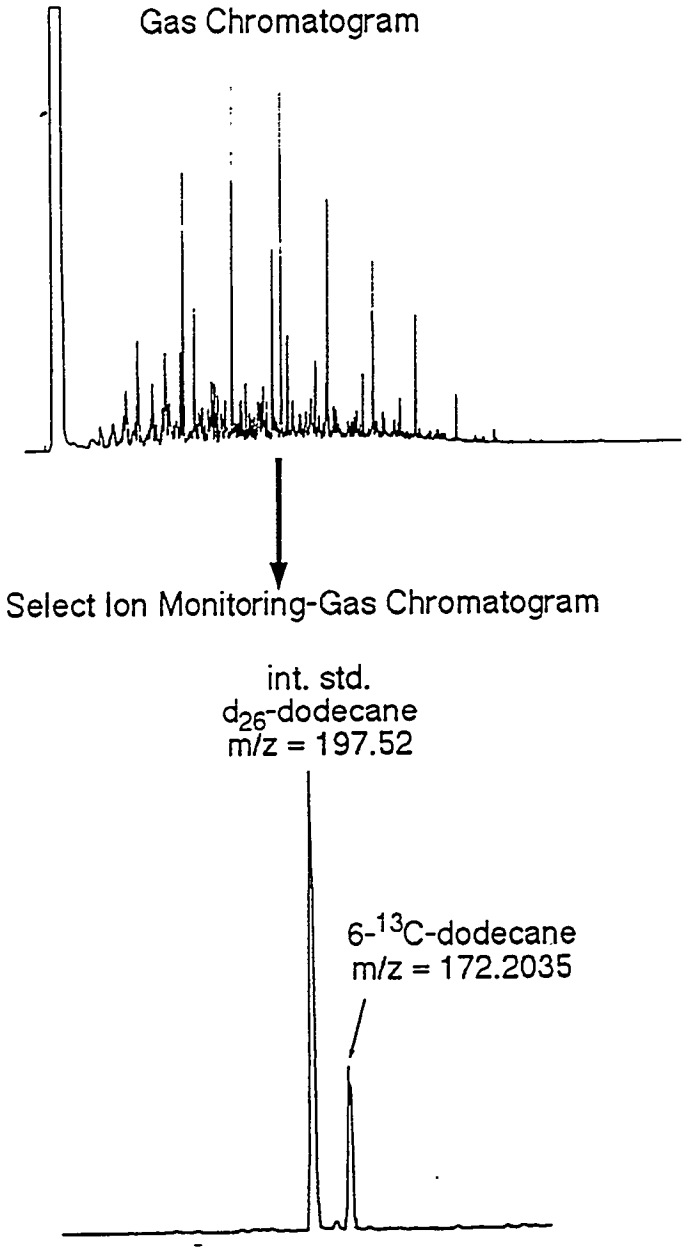

Figure 15: Gas chromatogram of 6-^{13}C-dodecane mixed with JP-8P at a concentration of 0.5% by weight. In comparison, a select ion monitoring-gas chromatogram is shown at the bottom where the two ions of interest correspond to M+1 peak of the internal standard, d_{26}-dodecane, and the M+1 peak of 6-^{13}C-dodecane.

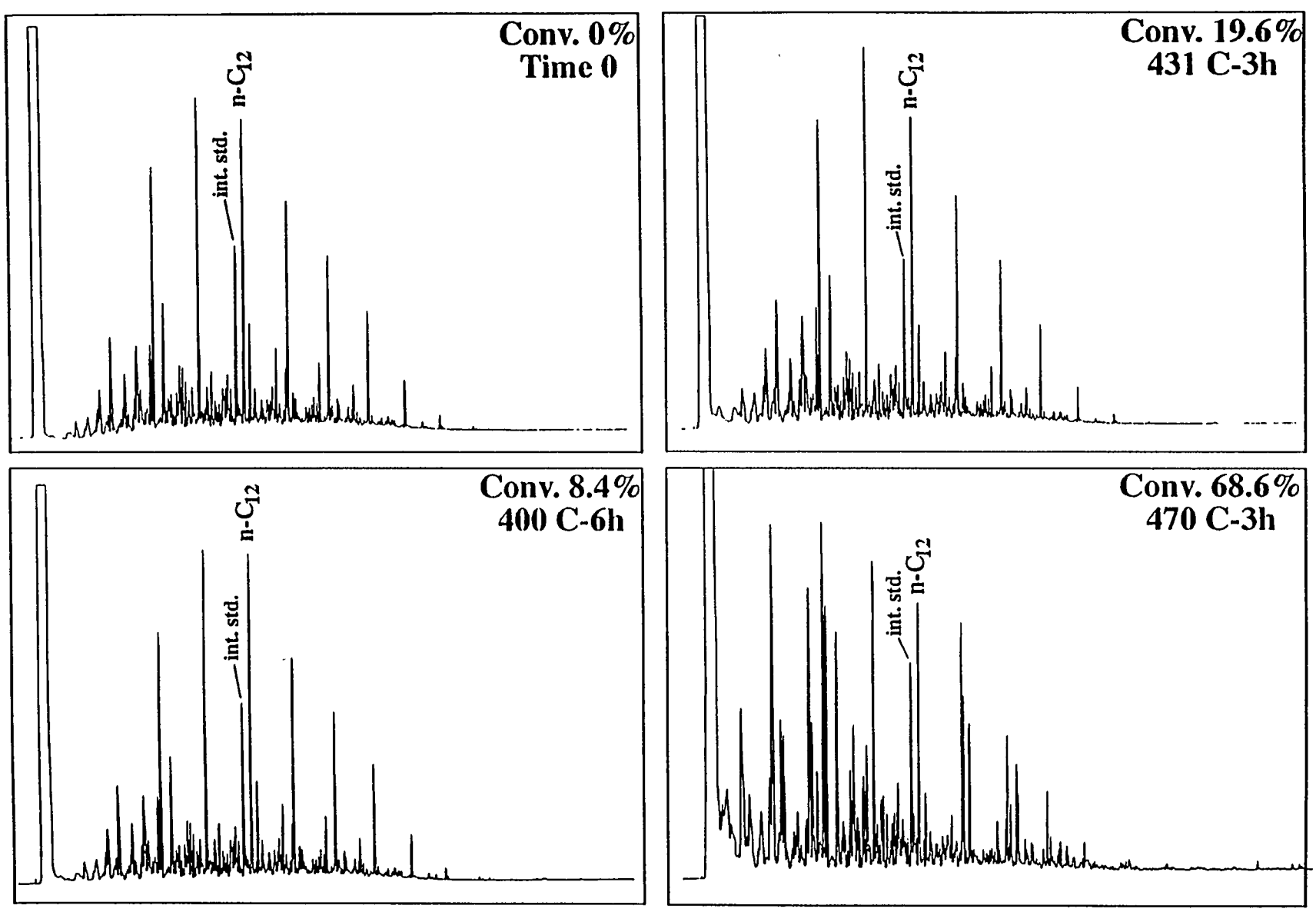

Figure 16: Gas chromatograms of 6-^{13}C-dodecane mixed with JP-8P heated at various temperatures and times. Conversion of 6-^{13}C-dodecane was determined by GC-SIMs.

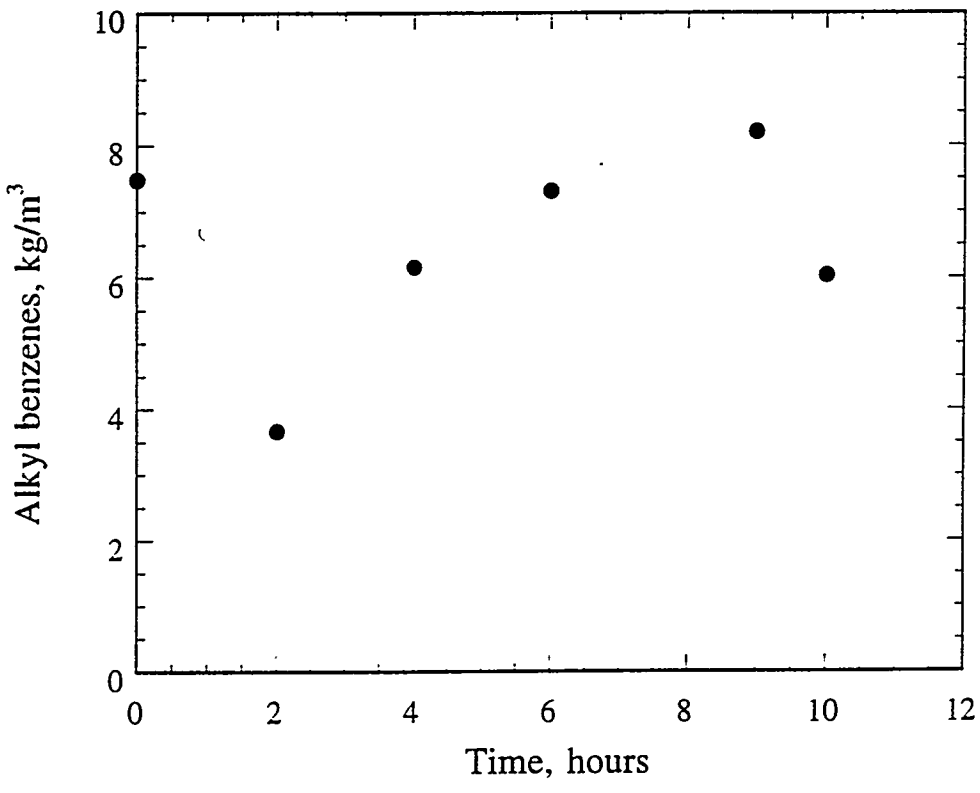

Figure 17 Concentration of substituted c3 and c4 alkyl benzenes obtained form 18.45% $C_{14}H_{30}$ in JP-8C at 450^{0}C in N_2 environment

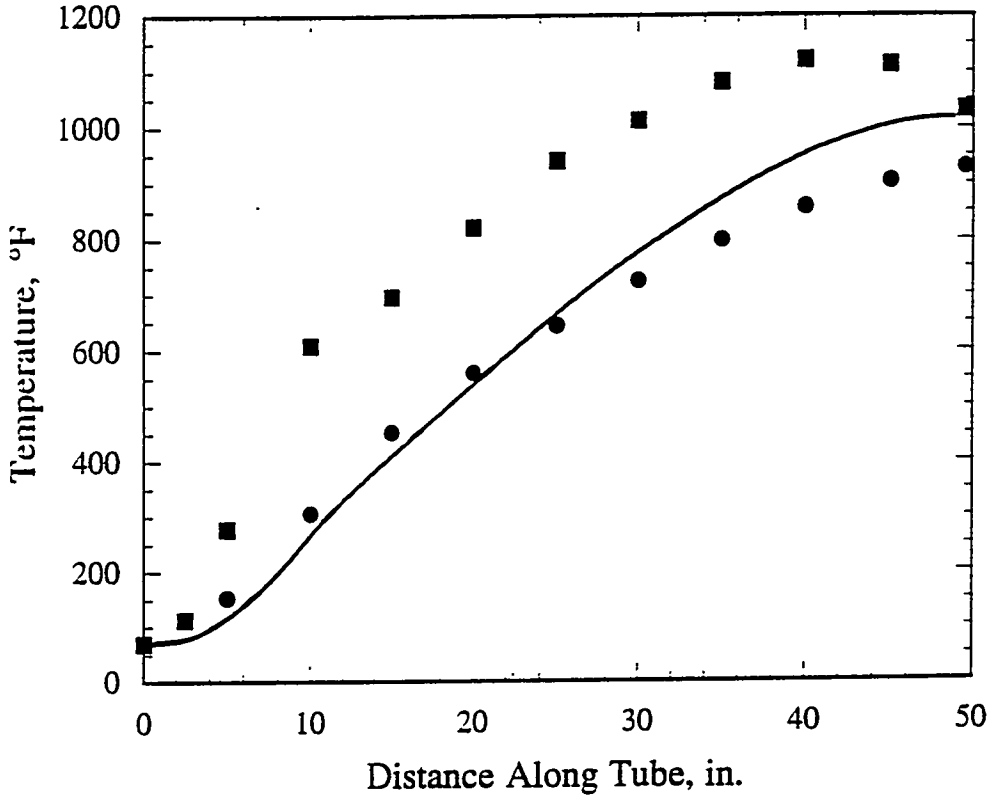

Figure 18. Comparison of STANTUBE mean fuel temperatures (—) with Wright Laboratory data for measured wall temperatures (■) and calculated mean fuel temperatures(●) .

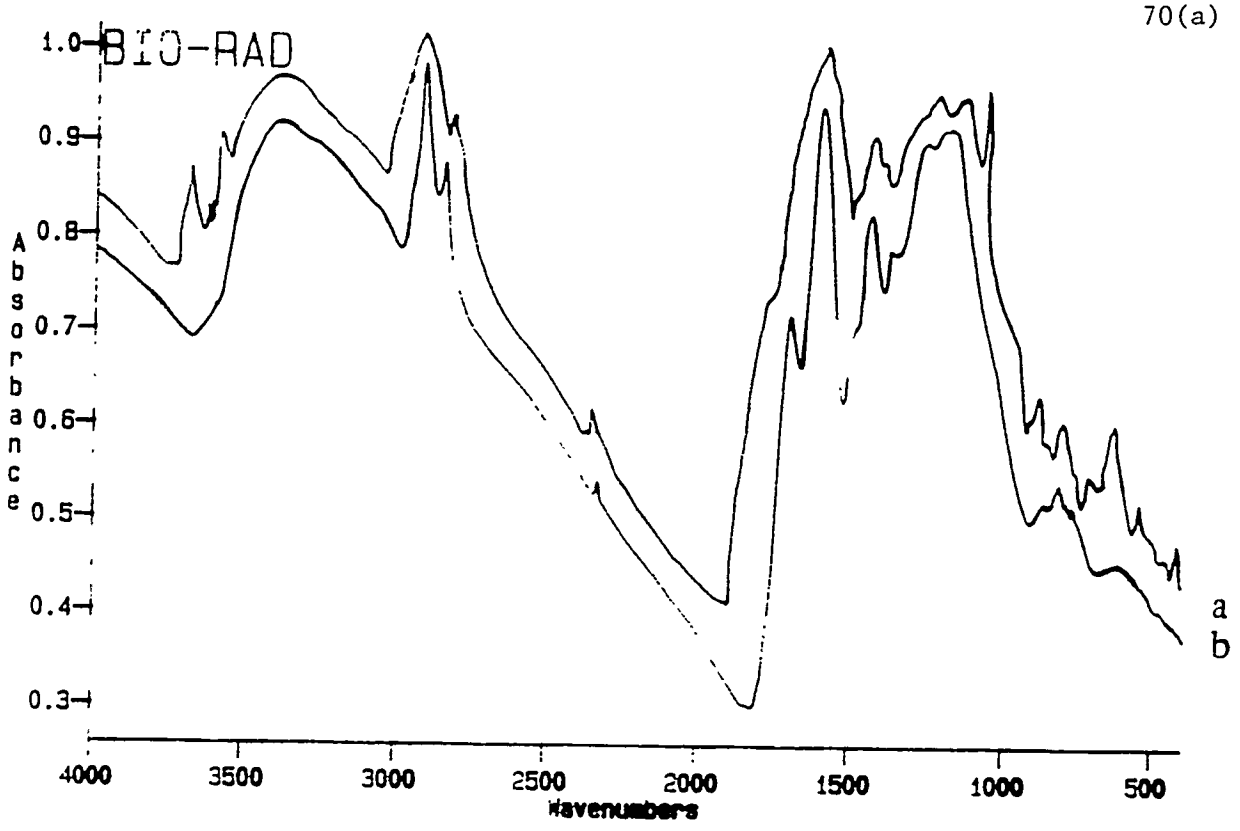

Figure 19. FTIR Spectra of (a) normal and (b) demineralised Wyodak Coal.

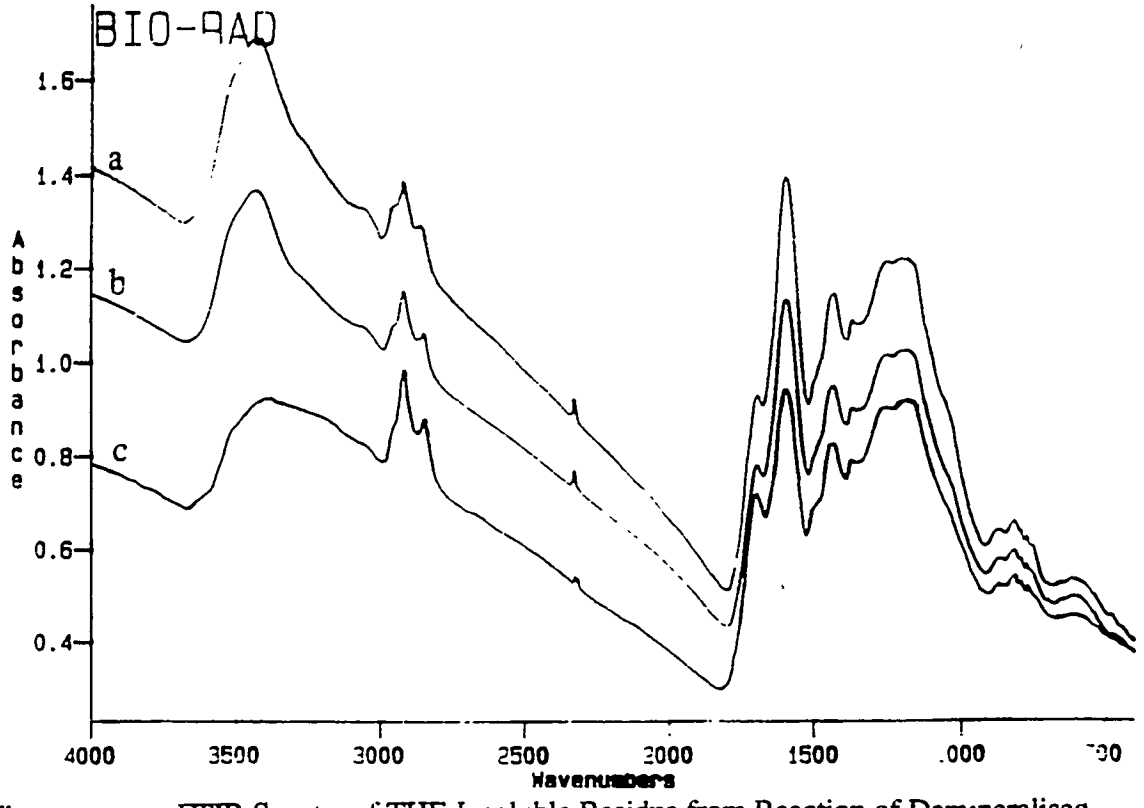

Figure 20. FTIR Spectra of THF-Insoluble Residue from Reaction of Demineralised Wyodak Coal in (a) Absence of Solvent, (b) Presence of Tetralin and (c) Presence of 1-MN.

APPENDIX III

CORRECTIONS FROM TRP #14

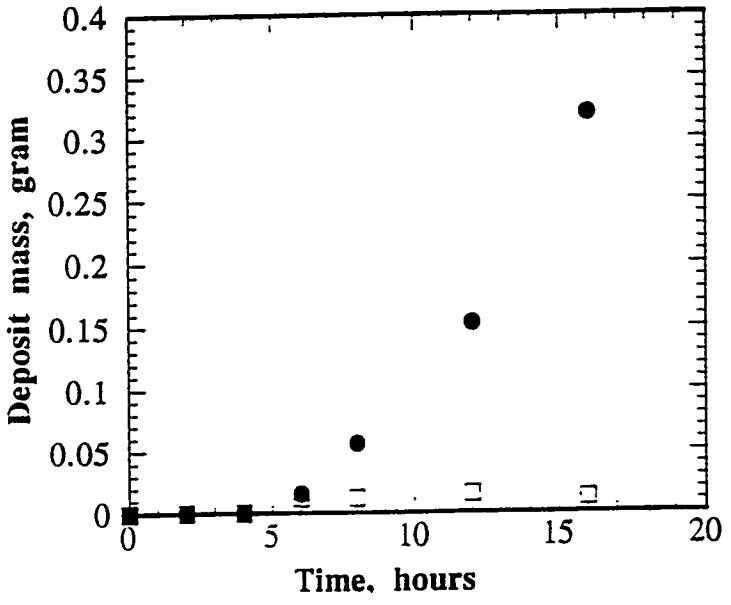

Fig. 13 Mass of deposit formed on the wall (●) and formed in the bulk (□) versus time.

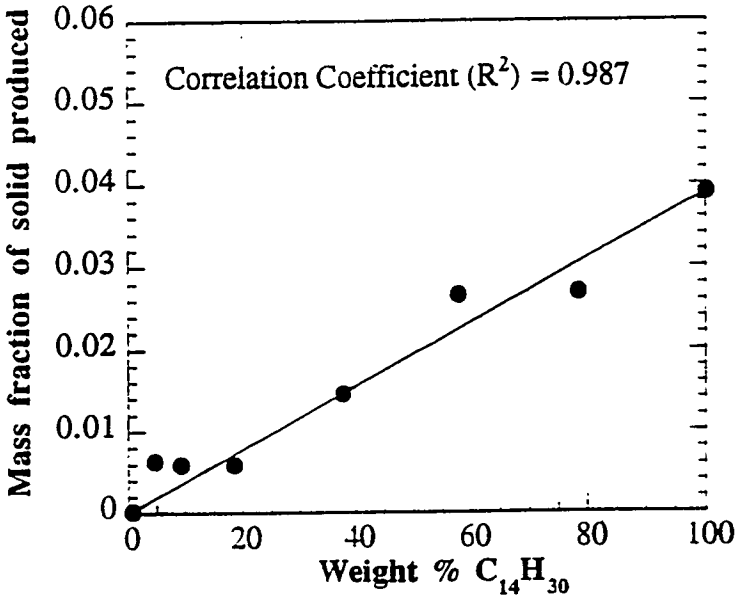

Fig. 14 Mass fraction of solid produced versus initial weight% of tetradecane (●). Linear regression with $r^2 = 0.987$ (—).

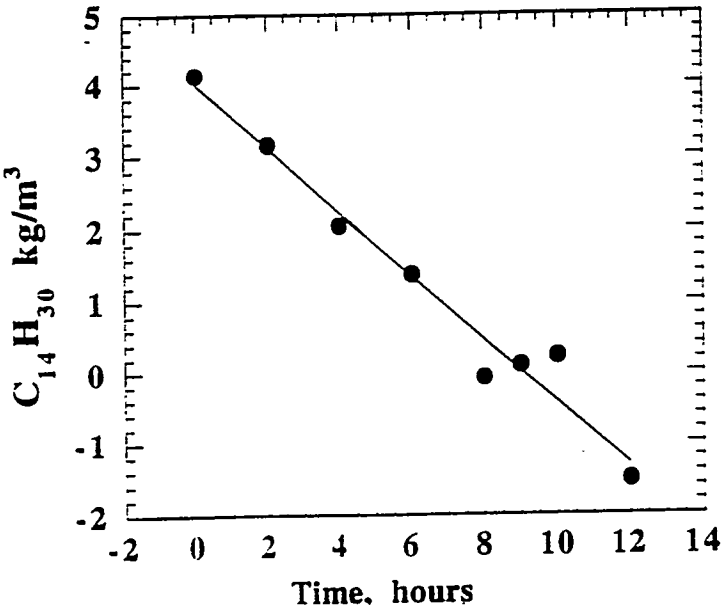

Fig. 15 Concentration of tetradecane (●) plotted versus time. Linear regression with r^2 = 0.984 (—).

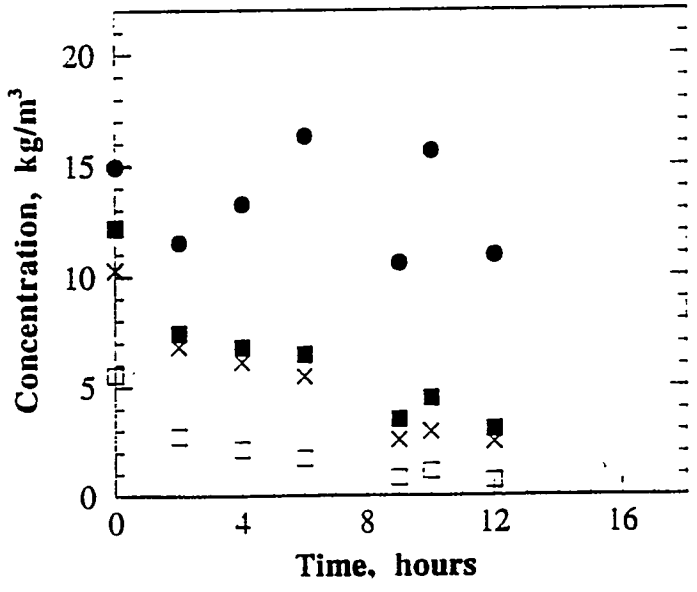

Fig. 16 Concentration, Methyl cyclohexane (●), ethyl cyclohexane (■), propyl cyclohexane (□), ethyl-methyl cyclohexane (×) versus time.

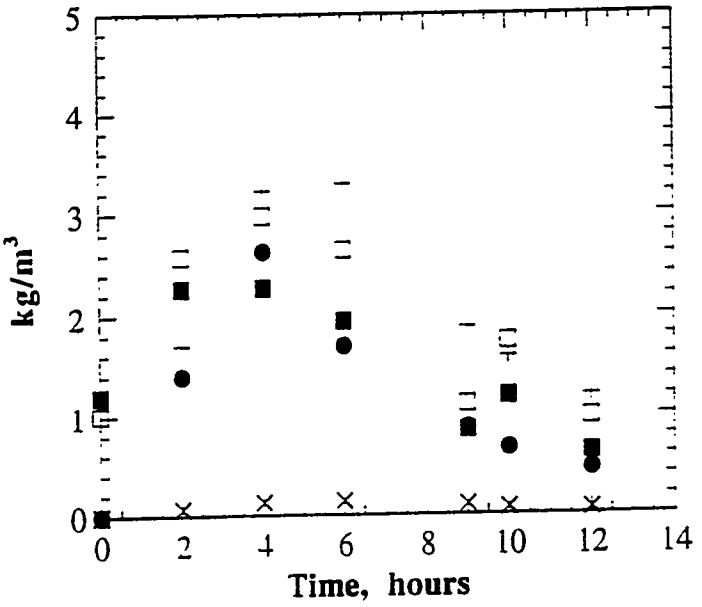

Fig. 17 Concentration of octane (●), nonane (□), decane (■), hexane (×), heptane (+), versus time.

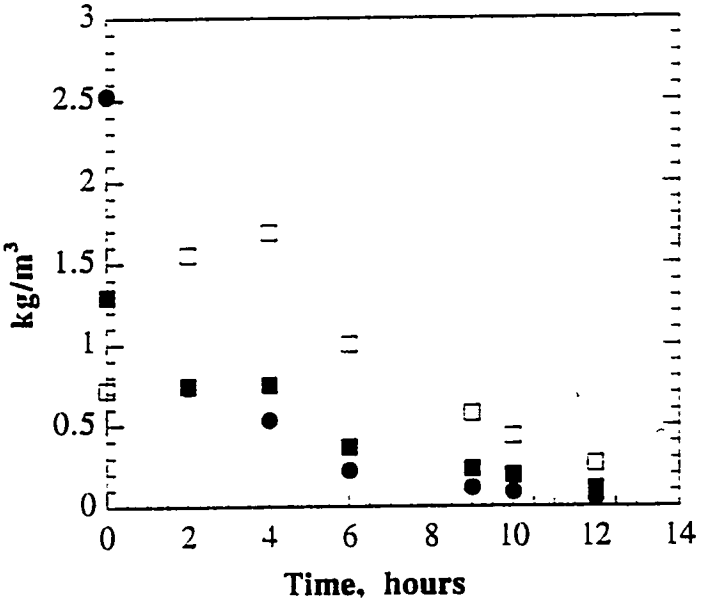

Fig. 18 Concentration of tridecane (●), dodecane (■), undecane (□), versus time.

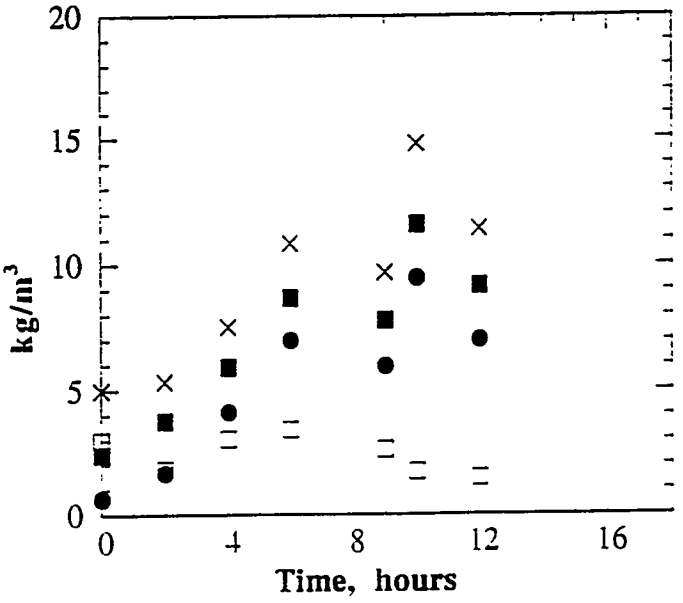

Fig. 19 Concentration of methylcyclopentane (●), cyclohexane (□), toluene (■), xylenes + ethyl benzene (×) versus time.

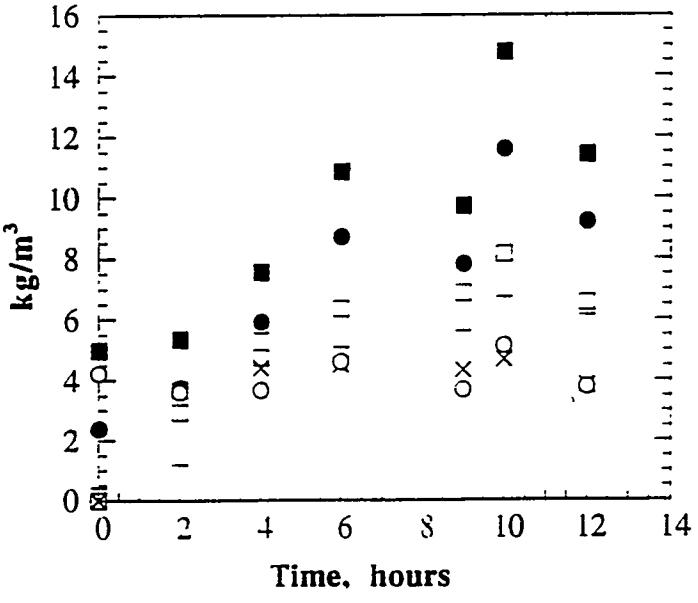

Fig. 20 Concentration of toluene (●), xylenes + ethyl benzene (■), naphthalene c1 (□), naphthalene c2 (×), naphthalene(+), indan c1 (○) versus time.

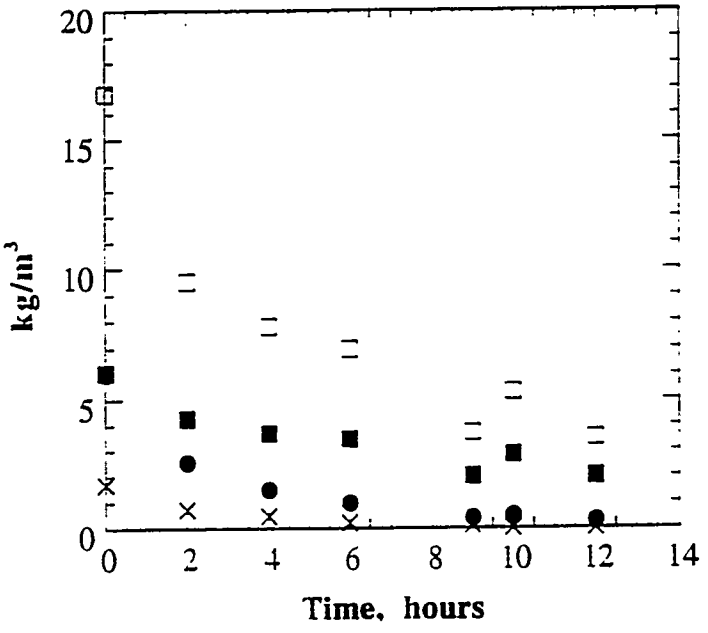

Fig. 21 Concentration of tetralin (●), decalin c1 (■), decalin (□), tetralin c1 (×) versus time.

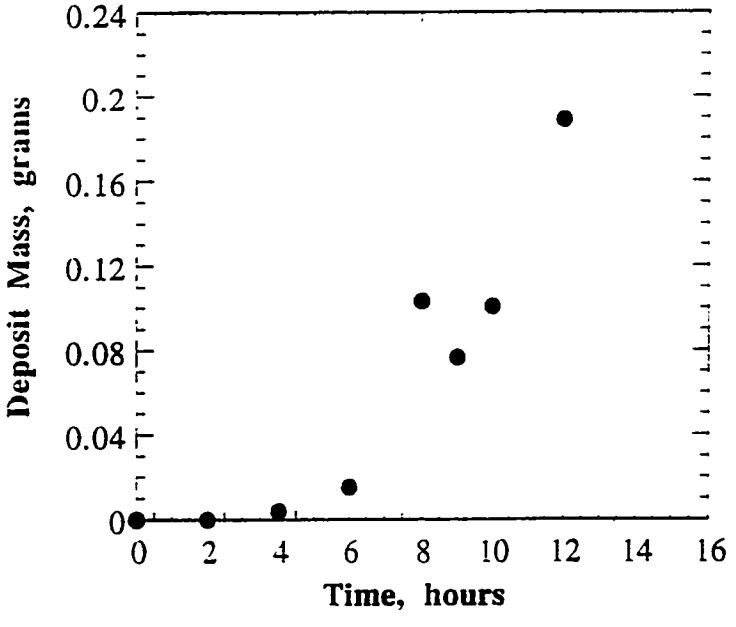

Figure 22. Deposit mass produced versus time.